University of Tennessee at Chattanooga
2024 Spring Research and Arts Conference

DOI 10.13140/RG.2.2.18572.08320

Analysis of Vibratory Pile Drivers using Longitudinal and Rotational Oscillations with a Purely Plastic Soil Model

Don C. Warrington, PhD., P.E.
University of Tennessee at Chattanooga
Department of Mechanical Engineering

Driving piles by longitudinal vibrations has been a proven technology since the Gorky dam project in the late 1940's. Shortly after that drivers which included both longitudinal and rotational oscillations were developed for driving tubular piles, both steel and concrete. Recent renewed interest in this technology for large offshore piles has occasioned the re-examination of the analysis of these piles using methods similar to those that Soviet developers used. In this paper a purely plastic model for both shaft and toe resistance is used parametrically to analyse the performance of these machines. Starting with the free-hanging case of no resistance with or without the effect of gravity, a dimensionless, parametric model was developed to analyse the system. Comparison with earlier analyses of a similar kind is included. The results shown an improvement in the movement of the pile per rotation of the eccentrics but further work needs to be done with improved soil modelling for more conclusive results.

Keywords: vibratory drivers, longitudinal oscillations, rotational oscillations, gentle pile driving, Soviet

Introduction

Vibratory driving of piles has been successfully performed since the original application at the Gorky hydroelectric facility in 1949 (Barkan (1957).) A comprehensive treatment of the development of that machine and the subsequent development of the technology in the decade that followed can be found in Savinov and Luskin (1960). That development included impact-vibration hammers, which were additionally discussed in D. Warrington and Erofeev (1995). The cycle analysis of these hammers was re-examined in D. Warrington (2023).

In 1952 M.G. Tseitlin, along O.A. Savinov and A. Ya. Luskin, proposed a vibratory driver which took the technology in a different direction: the inclusion of rotational oscillations in addition to longitudinal ones (Savinov and Luskin (1960).) They were able to demonstrate more effective driving using such a machine for axisymmetric piles such as pipes and concrete cylinder piles. The following year Tseitlin obtained an author's certificate for a machine which embodied this concept; this machine was built and tested with positive results. The machine is depicted in Figure 1.

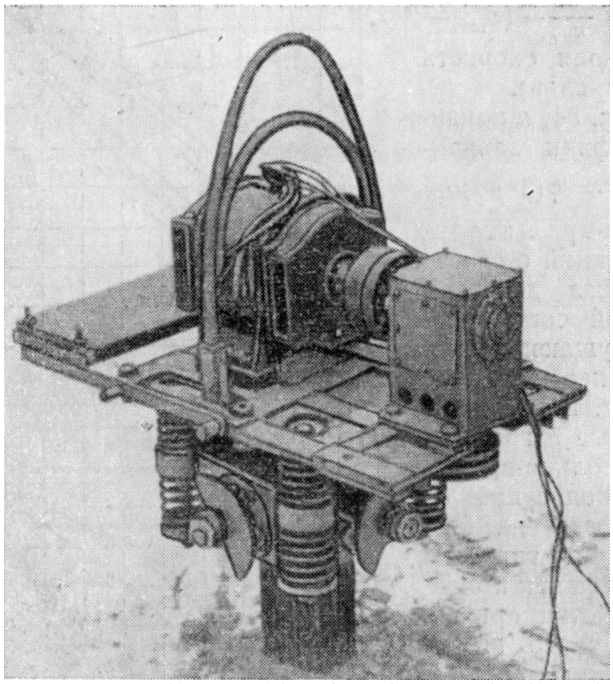

Figure 1. VKD vibratory driver for axisymmetric piles using both longitudinal and rotational oscillations (from Savinov and Luskin (1960))

The machine was used with piles ranging from 120 to 237 mm in diameter, and it was determined that the sinking speed

This work is dedicated to Mikhail Gregorovitch Tseitlin. The longitudinal-rotational vibratory driver was his life's work and its continuation is one of the objects of this research. It is important to remember that, when advances in technology take place, they do so built on that which has gone before, and it is important to acknowledge the previous work.

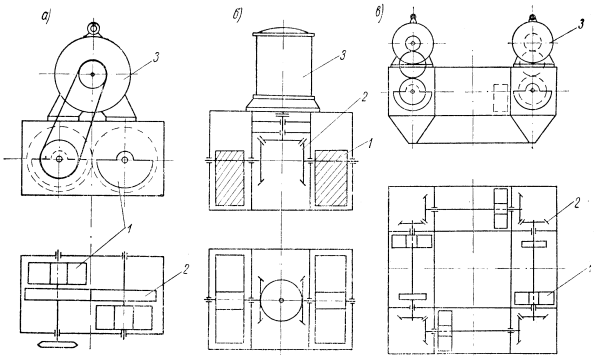

Figure 2. Diagrams of arrangements of vibratory drivers using both longitudinal and rotational oscillations. Left: two-shaft arrangement with parallel shafts. Centre: two shaft arrangement with coaxial shafts. Right: four shaft arrangement. Key: 1) eccentrics, 2) gears, 3) motors. (From Savinov and Luskin (1960))

of the pile was higher than a comparable driver using only longitudinal vibrations. It was also determined that the hammer used less energy than a driver without rotational oscillations.

Subsequent to this success drivers of this principle were proposed. An overview of different schemes of eccentric arrangement and power transmission is shown in Figure 2.

It is easy to see from Figure 2 that the guiding principle is simply to offset the eccentrics from the centre axis of the machine. Traditionally, with vibratory drivers the eccentrics have their axial centroids along the same centre axis; in this way the horizontal vibrations are offset and the vertical ones are added. With this type of machine we have eccentricity to produce both vertical and rotational oscillations.

One early decision in the design of these machines was how to phase the eccentrics. Depending on how the eccentrics are installed relative to the gear mesh, the differential phase angle between these oscillations can be varied. Experiments early in the development showed that a phase angle between the peak longitudinal and peak rotational oscillations of 90° was most advantageous for efficient driving. This arrangement had an additional advantage in that, during assembly, the eccentrics at rest were directly below the shafts, as is the case with conventional vibratory drivers. The Soviets referred to the driver that resulted as a "double-acting vibratory driver," an interesting choice of nomenclature for designers of impact pile driving equipment.

In spite of the efforts of its principal developer (Tseitlin (1969); Tseitlin, Verstov, and Azbel (1987)) there was little progress in this technology after its initial implementation. Recently interest in this type of machine has been revived by the installation of monopiles for offshore wind farms, and such machines have been built and tested (Tsetas et al. (2023).) One interesting change in this last machine, however, is that the frequency of the rotational oscillations is not the same as the longitudinal ones; they are generated by separate eccentric and motor systems. However, in this paper the original Soviet concept of one set of eccentrics operating at the same frequency for both types of oscillations will be maintained, as it may be advantageous for smaller and more economic machines.

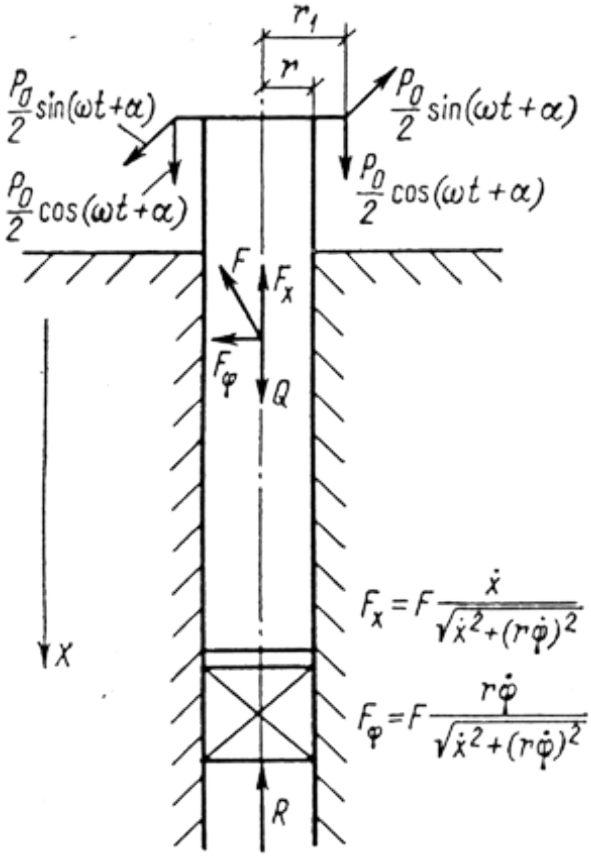

Figure 3. Force diagram for axisymmetric pile using both longitudinal and rotational oscillations (from Tseitlin et al. (1987))

Development of the Equations of Motion

Although many formulations of the equations of motion involved elliptical integrals and other mathematical formulations (Savinov and Luskin (1960); Tseitlin (1969); Tseitlin et al. (1987),) the model presented here is that of Tseitlin et al. (1987), which in terms of longitudinal vibrations has the same equations of motion as that reconstructed by D. Warrington (2021). The addition of rotational oscillations, however, complicates the analysis to a considerable degree, as will become evident. The model is shown in schematic form in Figure 3.

The equations of motion for this system are (Tseitlin et al. (1987))

$$m\frac{d^2}{dt^2}x(t) = P_o\,\cos(\omega\,t+\alpha) + Q - \frac{F\,\frac{d}{dt}x(t)}{\sqrt{\left(\frac{d}{dt}x(t)\right)^2 + r^2\left(\frac{d}{dt}\phi(t)\right)^2}} - n_{con}\,R \quad (1)$$

and

$$I_0\,\frac{d^2}{dt^2}\phi(t) = P_o\,r_1\,\sin(\omega\,t+\alpha) - \frac{F r^2\,\frac{d}{dt}\phi(t)}{\sqrt{\left(\frac{d}{dt}x(t)\right)^2 + r^2\left(\frac{d}{dt}\phi(t)\right)^2}} - n_{con}\,R f_f\,r Sign(\frac{d}{dt}\phi(t)) \quad (2)$$

There are two important things to note about these equations:

1. These equations are similar to those of D. Warrington (2022), as they both involve mass and rotational inertia; however, they are not coupled in the same way. It is thus possible to integrate these without having to first isolate the second derivatives by solving for them. We also will assume a constant rotational velocity, which further simplifies our analysis; the results of D. Warrington (2022) showed that this was a reasonable assumption for most vibratory drivers currently constructed.

2. For Equation (2), the sign function results in the following:

$$\begin{aligned}
&\frac{d}{dt}\phi(t) > 0, \text{Sign}(\frac{d}{dt}\phi(t)) = 1\\
&\frac{d}{dt}\phi(t) = 0, \text{Sign}(\frac{d}{dt}\phi(t)) = 0\\
&\frac{d}{dt}\phi(t) < 0, \text{Sign}(\frac{d}{dt}\phi(t)) = -1
\end{aligned} \quad (3)$$

It is easier to follow the development by first considering simplified cases, as was done in D. Warrington (2021, 2022).

Case 1: No External Forces

If $Q = F = R = 0$ is assumed, Equations (1) and (2) reduce to

$$m\frac{d^2}{dt^2}x(t) = P_o\,\cos(\omega\,t+\alpha) \quad (4)$$

and

$$I_0\,\frac{d^2}{dt^2}\phi(t) = P_o\,r_1\,\sin(\omega\,t+\alpha) \quad (5)$$

It can be noted that Equations (4) and (5) are independent of each other. At this point we make several changes in variables, some of which were discussed in D. Warrington (2021). These are as follows:

$$\tau = \omega\,t \quad (6)$$

$$\bar{x}(\tau) = x(t) \quad (7)$$

$$\bar{\phi}(\tau) = \phi(t) \quad (8)$$

$$X(\tau) = \frac{\bar{x}(\tau)m\omega^2}{P_o} \quad (9)$$

$$\Phi(\tau) = \frac{\bar{\phi}(\tau)I_0\,\omega^2}{P_0\,r_1} \quad (10)$$

Applying Equations (6), (7), (8), (9), and (10) to Equations (4) and (5) yield

$$\frac{d^2}{d\tau^2}X(\tau) = \cos(\tau+\alpha) \quad (11)$$

and

$$\frac{d^2}{d\tau^2}\Phi(\tau) = \sin(\tau+\alpha) \quad (12)$$

The solution of these equations is

$$X(\tau) = -\cos(\tau+\alpha) + C_1 + C_2\,\tau \quad (13)$$

and

$$\Phi(\tau) = -\sin(\tau+\alpha) + C_3 + C_4\,\tau \quad (14)$$

At this point two observations can be made to assist in solving for the constants.

The first one is that the initial displacements are a function of the coordinate system, i.e., the origin can be set arbitrarily without affecting the other results. For simplicity we assume that, for each cycle, the motion begins at the origin of the coordinate system, i.e., $X(0) = \Phi(0) = 0$. Doing this yields

$$X(\tau) = -\cos(\tau+\alpha) + \cos(\alpha) + (v_0 - \sin(\alpha))\,\tau \quad (15)$$

and

$$\Phi(\tau) = -\sin(\tau+\alpha) + \sin(\alpha) + \left(\frac{d}{d\tau}\Phi(0) + \cos(\alpha)\right)\tau \quad (16)$$

The second observation is that the last term of Equations (13) and (14) creates an unbounded condition unless the constants $C_2 = C_4 = 0$. This is because the solution must be periodic. This requirement can be achieved if $v_0 = \frac{d}{d\tau}X(0) = \sin(\alpha)$ and $\frac{d}{d\tau}\Phi(0) = -\cos(\alpha)$.

Additionally, if the phase angle is assumed to be $\alpha = \frac{\pi}{2}$, $v_0 = 1$ and $\frac{d}{d\tau}\Phi(0) = 0$. Equations (15) and (16) and their derivatives are plotted assuming these conditions in Figure 4. The results for $X(\tau)$ and $\frac{d}{d\tau}\Phi(\tau)$ are identical.

It is worth noting that, starting with

$$P_o = K\omega^2 \quad (17)$$

that Equations (9) and (10) can be reduced to

$$X(\tau) = \frac{\bar{x}(\tau)m}{K} \quad (18)$$

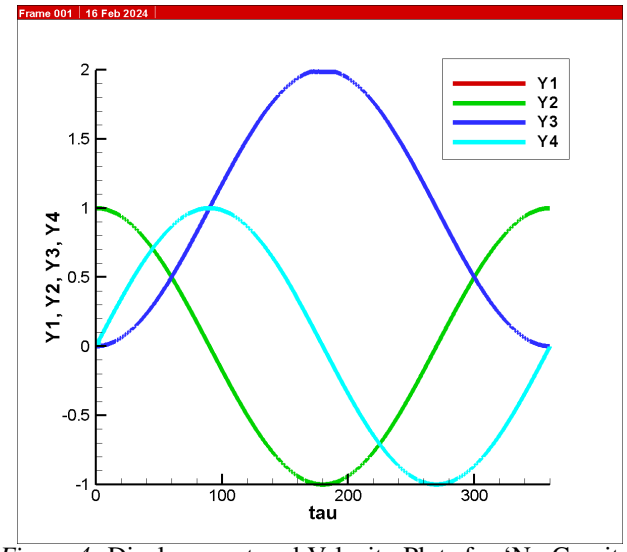

Figure 4. Displacement and Velocity Plots for 'No Gravity' Case

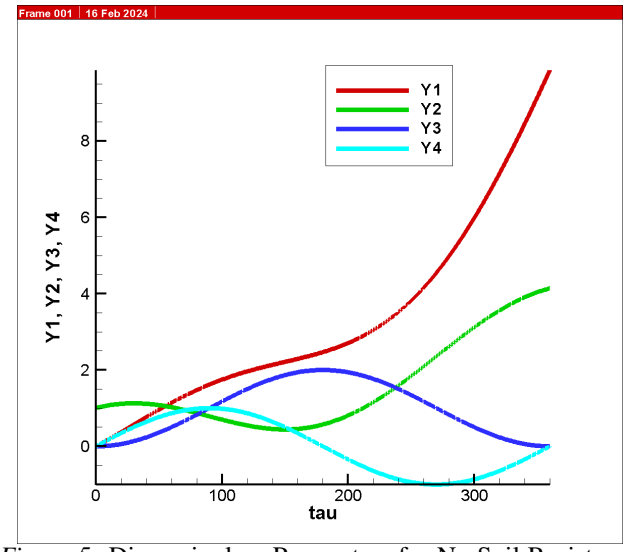

Figure 5. Dimensionless Parameters for No Soil Resistance and $q = 0.5,\ \alpha = \frac{\pi}{2}$

$$\Phi(\tau) = \frac{\bar{\phi}(\tau) I_0}{K\, r_1} \tag{19}$$

If the following is defined

$$A = \frac{K}{m} \tag{20}$$

and

$$A_1 = \frac{K r_1}{I_0} \tag{21}$$

Equations (18) and (19) become

$$X(\tau) = \frac{\bar{x}(\tau)}{A} \tag{22}$$

$$\Phi(\tau) = \frac{\bar{\phi}(\tau)}{A_1} \tag{23}$$

The variables A and A_1 are the "half-amplitudes" of longitudinal and rotational oscillations of the pile in its "free-hanging" state. These parameters can be used to relate the results of parametric studies to actual equipment configurations.

Case 2: Effect of the system weight without soil resistance

If we only include the system weight Q to Equation (1), we obtain

$$m\frac{d^2}{dt^2}x(t) = P_o\, \cos(\omega\, t + \alpha) + Q \tag{24}$$

No changes take place to the equation of motion for rotation. Applying the variable changes as before, and additionally

$$q = \frac{Q}{P_o} \tag{25}$$

the solution is

$$X(\tau) = -\cos(\tau)\cos(\alpha) + \sin(\tau)\sin(\alpha) + 1/2\, q\tau^2 + C_1 + C_2\, \tau \tag{26}$$

and its derivative

$$\frac{d}{d\tau}X(\tau) = \sin(\tau)\cos(\alpha) + \cos(\tau)\sin(\alpha) + q\tau + C_2 \tag{27}$$

For this case an unbounded solution cannot be avoided. This is sensible since, with no resistance to the downward force of gravity, the system will experience free-fall in a vacuum. Using $\tau = 0$ to solve the constants and differentiating for the velocity, the constants can be solved for and the equation becomes

$$X(\tau) = -\cos(\tau)\cos(\alpha) + \sin(\tau)\sin(\alpha) + 1/2\, q\tau^2 + \cos(\alpha) + (v_0 - \sin(\alpha))\, \tau \tag{28}$$

and

$$\frac{d}{d\tau}X(\tau) = \sin(\tau)\cos(\alpha) + \cos(\tau)\sin(\alpha) + q\tau + v_0 - \sin(\alpha) \tag{29}$$

For these equations, the initial conditions are $X(0) = 0$ and $\frac{d}{d\tau}X(0) = v_0$. As before, $v_0 = 1$ when $\alpha = \frac{\pi}{2}$.

The problem we have now is that, at the end of the cycle, with $\alpha = \frac{\pi}{2}$ and $v_0 = 1$, $X(2\pi) = 2q\pi^2$ and $\frac{d}{d\tau}X(2\pi) = 1 + 2\, q\pi$. With the displacement, we can simply reset the coordinate axes to the origin for the next cycle. With the velocity, there is an increasing velocity with every cycle; the end velocity of the previous cycle becomes the initial condition of the new one. This can be seen in Figure 5 under the conditions shown.

When a vibratory driver reaches an equilibrium velocity, it is the equivalent of a terminal velocity in a fluid, at which point the resisting force of the fluid is equal to the

weight/downward force of the system. The goal of analysing the system with soil resistance is to find the state at which a) the advance of the system per cycle is constant, and by extension the overall sinking velocity and b) the state at which the velocity trace for each cycle is the same up to the condition where $\frac{d}{d\tau}X(0) = \frac{d}{d\tau}X(2\pi)$ for the system.

It is one of the greatest regrets of the whole vibratory driver history that an equivalent fluid viscosity, as posited by Barkan (1957), cannot be consistently related to the axial load resistance of the pile during use. But it is one of the many elusive quantities that have made this application a challenge. As Massarsch (2023) ruefully observed:

> The mechanism that can explain the efficiency of vibratory driving of piles and sheet piles into granular soils has yet to be fully understood.

This should be compared with Savinov and Luskin (1960), who, almost three quarters of a century previous to this, made the following observation, in comparing Barkan's hypothesis with those of Yu. I. Neimark and others:

> Without dwelling on the later studies of S. A. Osmakov [38], A. S. Golovachev [22], O. Ya. Shekhter [66] and others, which are very similar in formulation to the works of Yu. I. Neimark, we note that none of the existing theoretical works gives a complete solution of the problem under consideration.

Case 3: With Soil Resistance

As stated earlier, the equations of motion for this case are Equations (1) and (2). These assume a purely Coulombic plastic model for the soil. With the above warning re soil response to vibration in mind, a transformation of these equations can be done. Before that, some additional dimensionless quantities need to be defined, namely

$$f = \frac{F}{P_o} \tag{30}$$

$$\gamma = \frac{R}{P_o} \tag{31}$$

$$a = \frac{r}{r_1} \tag{32}$$

$$b = \frac{mar_1^2}{I_0} = \frac{mr_1 r}{I_0} \tag{33}$$

With these in hand, making the same kinds of transformations as before, the equations of motion become

$$\frac{d^2}{d\tau^2}X(\tau) = \cos(\tau+\alpha) + q - \frac{f\frac{d}{d\tau}X(\tau)}{\sqrt{\left(\frac{d}{d\tau}X(\tau)\right)^2 + \left(\frac{d}{d\tau}\Phi(\tau)\right)^2 b^2}} - n_{con}\,\gamma \tag{34}$$

$$\frac{d^2}{d\tau^2}\Phi(\tau) = \sin(\tau+\alpha) - \frac{fa\left(\frac{d}{d\tau}\Phi(\tau)\right)b}{\sqrt{\left(\frac{d}{d\tau}X(\tau)\right)^2 + \left(\frac{d}{d\tau}\Phi(\tau)\right)^2 b^2}} - n_{con}\,\gamma f_f\, a\mathrm{Sign}\left(\frac{\omega\left(\frac{d}{d\tau}\Phi(\tau)\right)Kr_1}{I_0}\right) \tag{35}$$

Unfortunately these do not lend themselves to a closed form solution. It is necessary to resort to a numerical solution of the problem.

Issues in formulating a solution

The solution of these equations is deceptively simple because of the nature of the physics of the problem, at the heart of which is the choice to use a purely plastic model both for the shaft and toe soil resistance. Although these issues are presented sequentially, in reality they were taken as a whole in the development of the model.

"Piecewise" vs. "Stepwise" solution

The solution of these equations in Tseitlin et al. (1987) (and the purely longitudinal case reconstructed by D. Warrington (2021)) employed the use of a "piecewise" solution by dividing up the cycle into distinct sections. The advantages of that solution scheme are as follows:

1. It is easier to sort out the different phases of shaft frictional and toe resistances, relegating the case where the soil resistance exceeded the dynamic force to "parking" phases.
2. It is computationally less expensive, in principle at least.

The downside of such a solution scheme is that, in order to fit the physics of motion into the scheme, certain assumptions had to be made which could be unachievable in reality. The most egregious of these was the minimum toe resistance coefficient γ_{min}, which meant that the toe resistance had to achieve a certain level in order for the model to work. While it is necessary for the soil resistance to exceed the downward force of the system weight in order to avoid model collapse (in physical terms the system would descend by the system weight without excitation) such a constraint is not enforceable for all possible cases.

Another issue with the piecewise solution concerned the "parking" areas, i.e those portions of the cycle where there is no movement of the system as the eccentrics rotate. It was necessary in the earlier studies for the machine to stop, i.e. $\frac{d}{d\tau}X(\tau) = 0$, when entering a parking area. In reality it is possible for the inertia of the mass–longitudinal or rotational–to allow continued motion even when the soil forces exceed the forces generated by the machine and pile. Tseitlin et al. (1987) recognised this problem by noting that "(i)t is possible for the system to stop at the top only if $\frac{dx}{dt} = \frac{d\phi}{dt} = 0$ and the resultant of the active forces is less than the force of friction..."

$$f > \sqrt{a^2 \left(\sin(\tau+\alpha)\right)^2 + \left(\cos(\tau+\alpha)\right)^2 + 2\,\cos(\tau+\alpha)q + q^2} \tag{36}$$

Equation (36) is modified from Tseitlin et al. (1987) to be expressed in the dimensionless/parametric quantities described above. The condition under which parking can take place is thus very complex. For example, it possible for the two velocities to be at zero points at different times.

Further complicating matters is the phase angle α. Ideally this should be the angle between the peak force of the longitudinal vibrations and the point at which the machine disengages from the toe soil plug. Tseitlin et al. (1987) define this as

$$\alpha = \arccos(q) \tag{37}$$

There is no reference here to any soil resistance, unlike the case in D. Warrington (2021). It seems that this is more of a suggestion than a hard and fast quantity, and other solutions to the phase angle problem would have to be found.

Given all of this, a "stepwise" solution was adopted. This allows Equations (34) and (35) to govern for the entire cycle without having to stop the cycle. The 'parking' issue was resolved by making the steps small enough so that the system could oscillate around a constant displacement when a true parking state was achieved–with very small velocities–until the dynamic force became large enough to resume movement of the system. Using small steps also enabled the model to more readily pick up changes in plasticity, a phenomenon discussed in a different context in D. C. Warrington (2016).

Ground Contact Variable and Rotational Friction

The equations as described in Tseitlin et al. (1987) were set up for a piecewise solution. In order to express these in a format suitable for a stepwise solution, it was necessary to address the variable contact with the soil toe plug. This was done by defining the contact variable n_{con}, which is an integer. The pile is in contact with the soil plug under the following conditions:

1. When the displacement is greater than zero. In the raising stage of the cycle, the displacement goes negative, and thus there is no contact.

2. When the pile toe advances into the plug. This takes places when the longitudinal velocity is greater than zero and the displacement is greater than that of the plug, which is accounted for at all times during the cycle.

This means that, when both of these conditions are met, $n_{con} = 1$; otherwise, $n_{con} = 0$. In the case of Equation (34), this simply means that the toe resistance is opposite to the direction of the velocity. In the case of Equation (35) when $n_{con} = 1$ the toe and toe soil make contact but do so torsionally, with the torsional friction resisting the rotational velocity. A resisting torque is assumed with a Coulombic friction factor f_f and the outside diameter of the pile r. Tseitlin et al. (1987) do not give a value for f_f; based on data in Navy (1986), $f_f = 0.4$ for steel piling. This can obviously be changed if the pipe is being used as a vibratory drill bit or if the pile is another material.

Implementing the Equations and Enabling Convergence

Equations (34) and (35) were solved for $0 \leq \tau \leq 2\pi$ using a similar solution as was used in D. Warrington (2022), namely a fourth-order Runge-Kutta method as described in Carnahan, Luther, and Wilkes (1969). This means that first we define the equations

$$\begin{aligned} Y_1 &= X(\tau) \\ Y_2 &= \frac{d}{d\tau} X(\tau) \\ Y_3 &= \Phi(\tau) \\ Y_4 &= \frac{d}{d\tau} \Phi(\tau) \end{aligned} \tag{38}$$

and

$$\begin{aligned} F_1 &= Y_2 \\ F_2 &= \frac{d^2}{d\tau^2} X(\tau) \\ F_3 &= Y_4 \\ F_4 &= \frac{d^2}{d\tau^2} \Phi(\tau) \end{aligned} \tag{39}$$

in which case Equations (34) and (35) can be written as

$$F_2 = \cos(\tau+\alpha) + q - \frac{f Y_2}{\sqrt{{Y_2}^2 + {Y_4}^2 b^2}} - n_{con}\,\gamma \tag{40}$$

$$F_4 = \sin(\tau+\alpha) - \frac{f a Y_4 b}{\sqrt{{Y_2}^2 + {Y_4}^2 b^2}} - n_{con}\,\gamma f_f\, a \mathrm{Sign}\left(\frac{\omega\, Y_4 K r_1}{I_0}\right) \tag{41}$$

One benefit of this formulation over D. Warrington (2022) is that it was unnecessary to solve the equations for F_2 and F_4, and the acceleration equations could be used without modification.

In D. Warrington (2022, 2023), the model was started and allowed to run until convergence was achieved. Although this approach is sound from a physical standpoint, from a mathematical standpoint there is no guarantee of convergence. To improve both the rate and certainty of convergence, optimisation software was employed so that, at each rotation the sum of the squares of both velocity and displacement traces would be the same as the previous iteration, thus driving the optimisation step difference for the

Euclidean sum of all four sums to zero. The software used to achieve this was UNCMIN, which is described in Dennis and Schnabel (1996); Schnabel, Koontz, and Weiss (1985). The weakness of this approach is that there was no guarantee that the initial conditions of velocity for the next cycle would be matched, although in general this did take place. End-cycle displacement matching was not an issue as the coordinate system was reset with each cycle, and in any case the goal of the system is to produce positive (downward) longitudinal displacement with each cycle.

Since the formulation of Equation (37) was deemed inadequate, early runs attempted to include the phase angle α as a variable to be optimised. Successive attempts to make this work did not succeed; however, it was determined that, as long as the phase angle results in a point which is reasonably close to the separation of the toe soil and the pile, results were generally consistent within the limitations of the model. Eventually Equation (37) was abandoned and a phase angle of $\alpha = \frac{\pi}{2}$ was used. This also proved satisfactory in regions where the model was optimal in its application.

Computing the power requirements

As noted in Tseitlin et al. (1987), the power required to sustain rotation of the eccentrics and impart energy for the downward motion of the pile is the sum of the power of the longitudinal force and the rotational torque, or

$$N_{tot} = N_{long} + N_{rot} \tag{42}$$

The power for longitudinal motion was derived in detail in D. Warrington (2021). The result was that the power was put into 'alpha' form, which was originally derived from viscous load assumptions but can be extended to Coulombic ones as well. The power is given by the equation

$$N_{long} = \alpha_1 \frac{K^2 \omega^3}{m} \tag{43}$$

Although α_1 is generally an expression of a complete vibratory cycle energy and power, D. Warrington (2021) notes that its computation can be broken up into stages, with the total α_1 being computed by summing the value of α_1 for all the stages. This is also the case with time steps, and the values for α_1 can be done in this way. It is thus necessary to enable the model to compute α_2 as well, starting with the viscous case. The derivation that follows parallels that of D. Warrington (2021).

Beginning with the governing equation of rotational torque (Tseitlin et al. (1987),)

$$N = \frac{\int P_o \, \sin(\omega t + \alpha) r_1 \, \frac{d}{dt}\phi(t) dt}{T} \tag{44}$$

Multiplying both sides by the period of oscillation, the energy per cycle is obtained. Additionally invoking Equation (17),

$$E_{cyc} = \int K\omega^2 \sin(\omega t + \alpha) r_1 \frac{d}{dt}\phi(t) dt \tag{45}$$

Making the substitutions from Equations (6) and (23),

$$E_{cyc} = \int \frac{\sin(\tau + \alpha) K^2 \omega^2 {r_1}^2 \frac{d}{d\tau}\Phi(\tau)}{I_0} d\tau \tag{46}$$

Collecting terms, a dimensionless cyclic energy can be defined thus:

$$E'_{cyc} = \frac{I_0 \, E_{cyc}}{K^2 \omega^2 {r_1}^2} = \int \sin(\tau + \alpha) \frac{d}{d\tau}\Phi(\tau) d\tau \tag{47}$$

Noting that α_2, like α_1, is first derived from viscous considerations, the equation of motion for rotary oscillations with viscous resistance is

$$I_0 \frac{d^2}{dt^2}\phi(t) + c_0 \frac{d}{dt}\phi(t) = K\omega^2 r_1 \, \sin(\omega t) \tag{48}$$

This is similar to the formulation given in D. Warrington (2006). The steady state solution of this equation (without the exponential term, which goes to zero as time progresses) is

$$\phi(t) = -\frac{\omega K r_1 \, (\cos(\omega t) c_0 + I_0 \, \omega \, \sin(\omega t))}{{c_0}^2 + \omega^2 {I_0}^2} + \frac{\omega K r_1}{c_0} \tag{49}$$

Defining

$$\xi = \frac{c_0}{\omega I_0} \tag{50}$$

this yields

$$\phi(t) = -\frac{K r_1 \left(\cos(\omega t)\xi^2 + \xi \, \sin(\omega t) - \xi^2 - 1\right)}{I_0 \, (\xi^2 + 1)\, \xi} \tag{51}$$

and the steady-state velocity is

$$\frac{d}{dt}\phi(t) = -\frac{K r_1 \left(-\sin(\omega t)\omega \xi^2 + \xi \, \cos(\omega t)\omega\right)}{I_0 \, (\xi^2 + 1)\, \xi} \tag{52}$$

Substituting this into Equation (45) and integrating results in

$$E_{cyc} = \frac{\omega^2 K^2 {r_1}^2 \xi \pi}{I_0 \, (\xi^2 + 1)} \tag{53}$$

Since

$$N = \omega E_{cyc} \tag{54}$$

the power for rotational oscillations with viscous resistance is thus

$$N = \frac{\xi}{2\left(\xi^2+1\right)} \frac{K^2\omega^3 {r_1}^2}{I_0} \tag{55}$$

For the viscous case, the definition of α_2 is

$$N = \alpha_2 = \frac{\xi}{2\left(\xi^2+1\right)} \tag{56}$$

The value of α_2 is at a maximum when $\xi = 1$, and $\alpha_2 = \frac{1}{4}$, the same as the longitudinal case.

More generally (and without the viscous assumption) the power can be computed as

$$N = \alpha_2 \frac{K^2\omega^3 {r_1}^2}{I_0} \tag{57}$$

and the energy per rotation is

$$E_{cyc} = \alpha_2 \frac{K^2\omega^2 {r_1}^2}{I_0} \tag{58}$$

Combining Equations (47) and (58) and solving for α_2,

$$\alpha_2 = \frac{E'_{cyc}}{2\pi} \tag{59}$$

The cyclic energy were computed stepwise for each time step using Equation (47) and then each result was converted to α_2. The results were summed for the entire cycle, at which point α_2 was computed for the entire rotation. A similar procedure was employed for computing α_1. The total power is thus

$$N_{tot} = N_{long} + N_{rot} = \alpha_1 \frac{K^2\omega^3}{m} + \alpha_2 \frac{K^2\omega^3 {r_1}^2}{I_0} \tag{60}$$

or, making other substitutions,

$$N_{tot} = \left(\alpha_1 + \alpha_2 \frac{b}{a}\right) \frac{K^2\omega^3}{m} = \alpha_{tot} \frac{K^2\omega^3}{m} \tag{61}$$

Unfortunately the two values of α_n do not directly add for all cases. However,

$$\alpha_{tot} = \alpha_1 + \alpha_2, \; a = b \tag{62}$$

The best condition for this to take place is if $a = b = 1$, which is reasonable because:

1. When $a = 1$ the radius of the pile is equal to the radius of the eccentric offset, which makes sense for the equipment to be of similar sizing to the pile being driven.

2. The condition $I_0 \approx mr_1^2$ is a crude approximation of the rotational moment of inertia, assuming the driver is the largest portion of that inertia. If $a = 1$, then for $I_0 \approx mr_1^2$ the condition in Equation (62) means that $b \approx 1$. This will be an important configuration in our analysis; due to variations in equipment configuration common in vibratory drivers (and especially considering the configurations shown in Figure 2) and piling, anticipating parameters such as a and b is difficult.

Table 1
Summary of the Results of Case Study, 1) from D. Warrington (2021), 2) current model, $a = b = 1$

Parameter	(1)	(2)
q	0.2	
f	0.5	
γ	1.0	
α, degrees	44.42700	79.577
$Y_{1_{max}}$	0.5133014	1.0736
α_1	0.1750364	0.34216
α_2	-	0.19745
y/α_{tot}	2.932541	1.98969

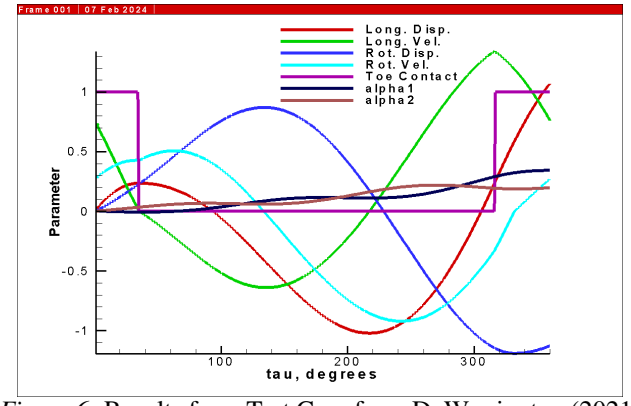

Figure 6. Results from Test Case from D. Warrington (2021)

Test Cases

Case 1: Single Test Case

The model developed, the first case to be presented is a repeat of D. Warrington (2021). In this case $f = 0.5$, $q = 0.2$, $\gamma = 1$, $a = b = 1$. Comparison of the results is shown in Table 1.

The cyclic results are shown graphically in Figure 6.

The following can be noted about the results:

1. The movement of the system for each cycle is nearly doubled.

2. The power requirement to accomplish this is more than doubled, so much so that the ratio of displacement per cycle and power decreases by a third.

3. The phase angle given for the current model in Table 1 is estimated from the point where the system separates from the toe, i.e., the toe contact variable n_{con} changes from 1 to 0. The model was actually run for a phase angle of $\alpha = 90°$. Earlier tests on the model show that the difference in the result is minimal for cases where the model is optimal.

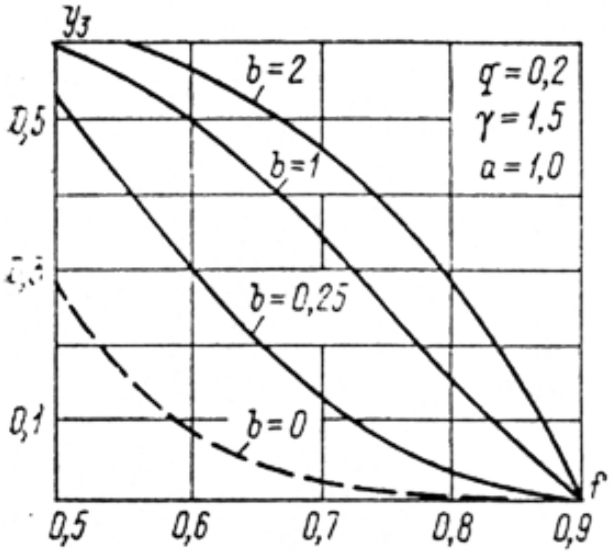

Figure 7. Survey of results for $Y(1)_{max}$ for various values of f and b (from Tseitlin et al. (1987))

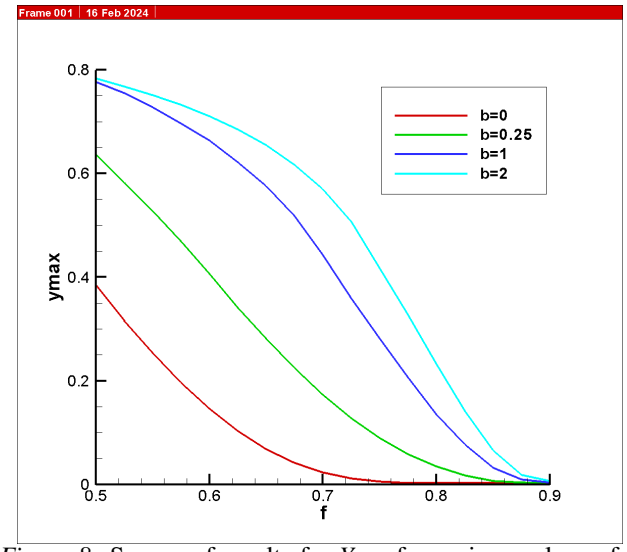

Figure 8. Survey of results for $Y_{1_{max}}$ for various values of f and b using the current model

4. The difference between the initial and final longitudinal velocity Y_2 is .0016753 and the initial and final rotational velocity Y_4 is -2.48×10^{-6}. As noted earlier, the method used to minimise the difference in the sums of the squares did not guarantee agreement at any specific point, including the beginning/end of the cycle, but these results are reasonable.

5. The values for α_1 and α_2 are cumulative for each time step. The result at the right hand side of the graph is the total value for each of these variables. It is worth noting that the eccentrics impart energy to the system on an alternating basis during the cycle. One of the difficulties in the way energy is transferred to the eccentrics during rotation in vibratory driving systems is the variable way this is done; the rotational inertia of the eccentrics is necessary (and generally successful, D. Warrington (2022)) in smoothing this out. The addition of energy transfer during the 'low' times may further improve this situation.

Case 2: Survey of the Effects of Rotational Inertia

In Tseitlin et al. (1987) there was conducted a survey of the effects of differing values of b, which represents the rotational inertia of the system. These are shown (with the other governing variables) in Figure 7. The results of the present model for the same parameters is shown in Figure 8.

Comparison of the results show that, although qualitatively the results are similar, quantitatively the model predicts higher displacements than those from Tseitlin et al. (1987). Additionally, as $f \rightarrow 0.9$, the result from Tseitlin et al. (1987) drops straight to zero while, in Figure 8, the result 'tapers off' to zero. Why the two are different is not clear, because the reference is not specific on a number of points regarding the implementation of their model. Some of the difficulties in this implementation, such as the phase angle and the way the model handled the parking issue, have already been discussed. It is entirely possible that, using the stepwise model implemented, the constraints caused by the piecewise model were eliminated, thus affecting the results. In both cases, however, when $f = 0.9$ the advance per cycle is basically over.

The case of $b = 0$ is assumed to be an attempt to replicate purely longitudinal oscillations. That being the case, for the case of $b = 0$, likewise $a = 0$ in order to completely eliminate any spurious effects (especially power consumption) that might spill over from the equations of rotational oscillation. In this way the current model was adapted to use with the purely longitudinal oscillation case.

Parametric Studies

These studies are more broad-based; the data for the test cases was taken from there. Running parametric studies produced a great deal of data; the examination of that data will be very selective. The range of cases for from which results were obtained were as follows:

- Range of soil and downward force combinations:
- $0 \leq f \leq 0.9$ (for all combinations of a and b)
- $0.025 \leq q \leq 0.975$ (for all combinations of a and b)
- $0.5 \leq \gamma \leq 2$ (for all combinations of a and b)
- Comparison of purely longitudinal oscillations with combined ones
- $a = 0$, $b = 0$ (replication of purely longitudinal oscillations)
- $a = 1$ $b = 1$ ('standard' case for combined vibratory action)
- Comparison of change of pile diameter

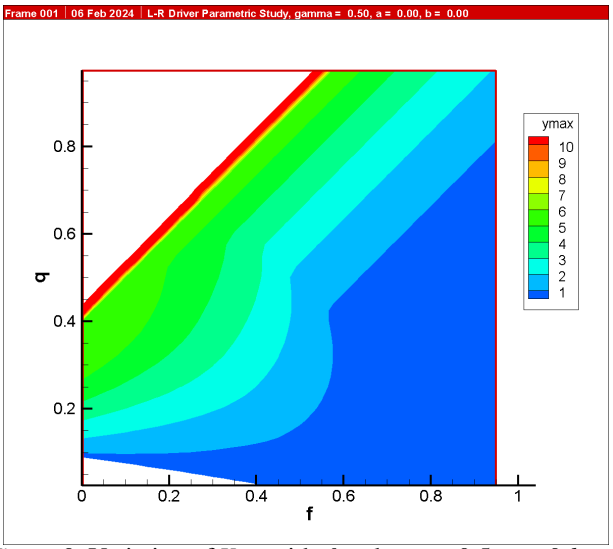

Figure 9. Variation of $Y_{1_{max}}$ with f and q, $\gamma = 0.5$, $a = 0$ $b = 0$

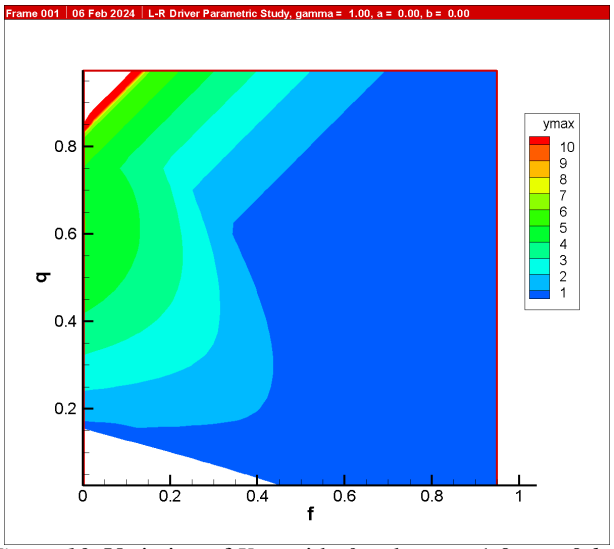

Figure 10. Variation of $Y_{1_{max}}$ with f and q, $\gamma = 1.0$, $a = 0$ $b = 0$

- $b = 1$ and $a = 0.5$ or $a = 1.5$
  - Comparison of change of system rotational inertia
- $a = 1$ and $b = 2$ or $b = 0.25$

The primary comparison will be the maximum displacement per cycle; power and displacement/power ratio will be considered only for the first comparison.

Comparison of purely longitudinal oscillations with combined ones

The simplest way to present the comparison of the two is in graphical format. The first comparison is the displacement for cases where a) $a = 0$, $b = 0$ and b) $a = 1$, $b = 1$. These results are shown for (a) in Figures 9-12 and for (b) in Figures 13-16.

From Figures 9-16 the following can be noted:

- The displacement of the system with each cycle is greater when rotational oscillations are included than when only longitudinal oscillations are considered.
- There are two areas which are in white which are explained as follows:
- The upper left hand corner is the region where the downward force of the system weight overcomes the combined shaft and toe resistance of the pile and the model collapses.
- The lower left and corner is the region where the downward force of the system is inadequate to move the system, in which case the model reported a net negative movement.
- Both of these phenomena are most pronounced for low values of f. The first one is most prominent for low values of γ and the second for high values of γ.
- One constraint of the model of D. Warrington (2021) was that of the 'diagonal,' i.e., the condition where

$$q + f = 1 \tag{63}$$

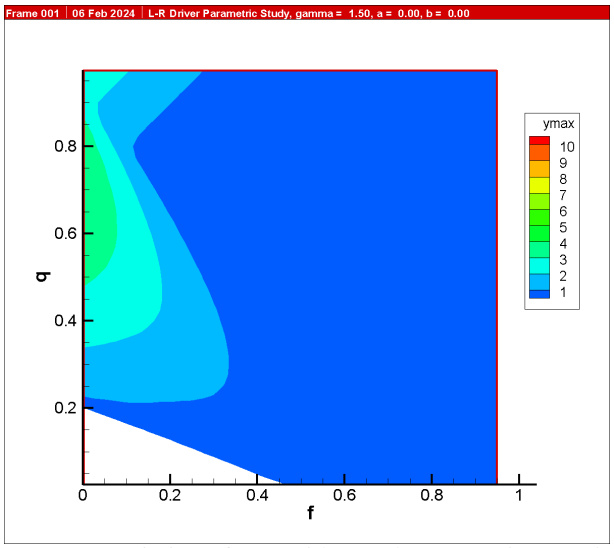

Figure 11. Variation of $Y_{1_{max}}$ with f and q, $\gamma = 1.5$, $a = 0$ $b = 0$

Above this line ($q + f \geq 1$) it was posited that static equilibrium would not permit the dynamic force to move the vibrator upward. The effect of this phenomenon is easier to see in the cases where $a = 0$ $b = 0$, i.e. Figures 9-12. Evidently the presence of rotational oscillations 'blurs' the diagonal and allows the machine to operate in a superior way in conditions where it was not optimal before. However, since additional movement was observed above the diagonal in both cases, using the stepwise model opens up the analysis of conditions which were not possible with the piecewise model.

- In both cases the optimal region for operation was the region between the diagonal and the region where inadequate

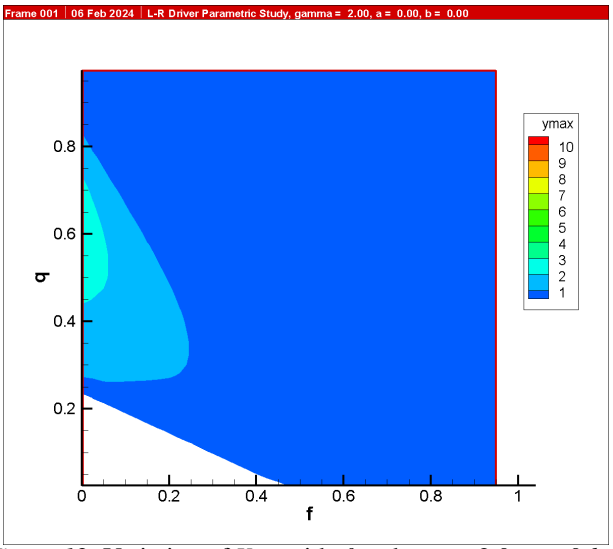

Figure 12. Variation of $Y_{1_{max}}$ with f and q, $\gamma = 2.0$, $a = 0$ $b = 0$

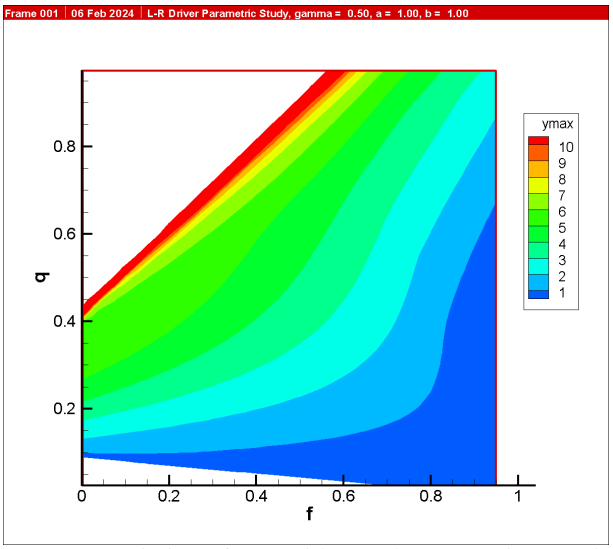

Figure 13. Variation of $Y_{1_{max}}$ with f and q, $\gamma = 0.5$, $a = 1$ $b = 1$

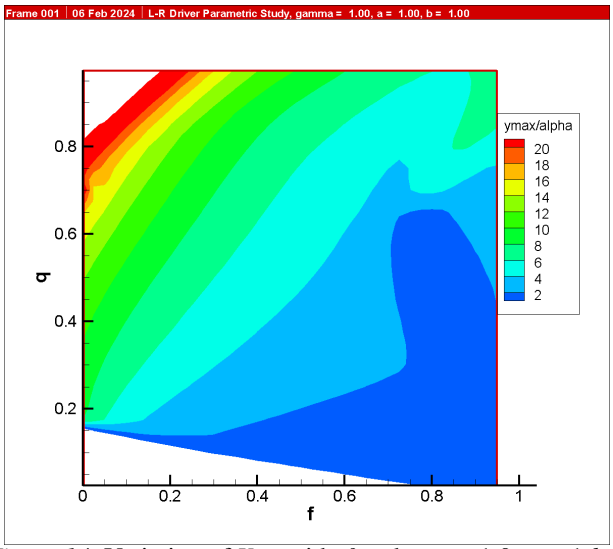

Figure 14. Variation of $Y_{1_{max}}$ with f and q, $\gamma = 1.0$, $a = 1$ $b = 1$

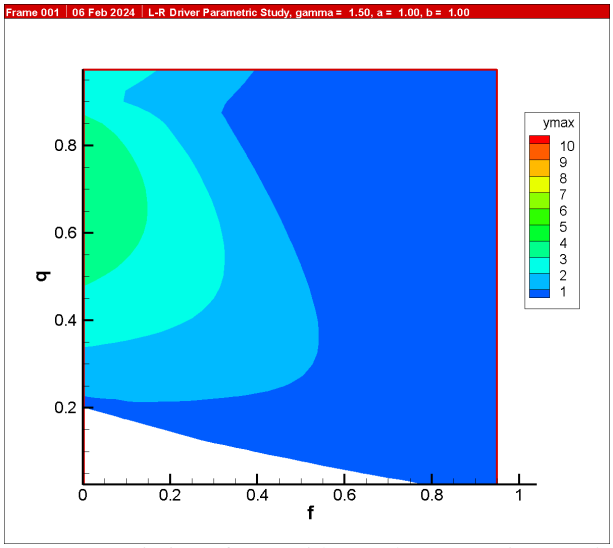

Figure 15. Variation of $Y_{1_{max}}$ with f and q, $\gamma = 1.5$, $a = 1$ $b = 1$

downward force prohibited the progress of the system.

Now the issue of power can be considered, and these results are shown in Figures 17-24.

Figures 17-24 show a) an increase in longitudinal power consumption with the inclusion of rotational oscillations and b) values of $\alpha_1 > \frac{1}{4}$, which is the upper limit using a purely viscous model of soil resistance. This phenomenon was discussed in D. Warrington (2021). These also show that power consumption increases with higher toe resistance, a major contributor to power consumption beyond purely viscous considerations.

Vibrators with both longitudinal and rotational vibrations consume power in two ways, in accordance with Equation (42). The results for α_2 for $a = 1$ $b = 1$ are shown in Figures 25-28.

Values for α_2 are lower than those for α_1. They also tend to 'ignore' the diagonal as well.

Next the graphs for $a = 0$ $b = 0$ and the ratio $\frac{Y_{1_{max}}}{\alpha_1}$ are presented in Figures 29-32.

It is worth noting that the diagonal is very pronounced in Figures 29-32, especially as γ increases.

Assuming the conditions for Equation (62) apply, we can add α_1 and α_2 directly, and so can present the same survey of $\frac{Y(1)_{max}}{\alpha_1+\alpha_2}$ for $a = 1$, $b = 1$, as shown in Figures 33-36.

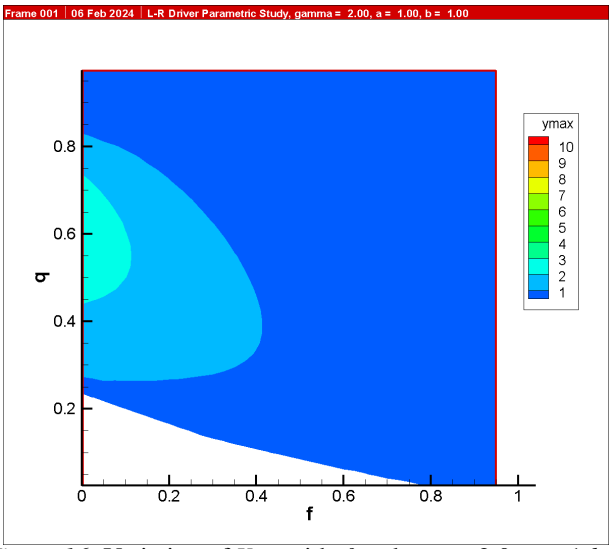

Figure 16. Variation of $Y_{1_{max}}$ with f and q, $\gamma = 2.0$, $a = 1$ $b = 1$

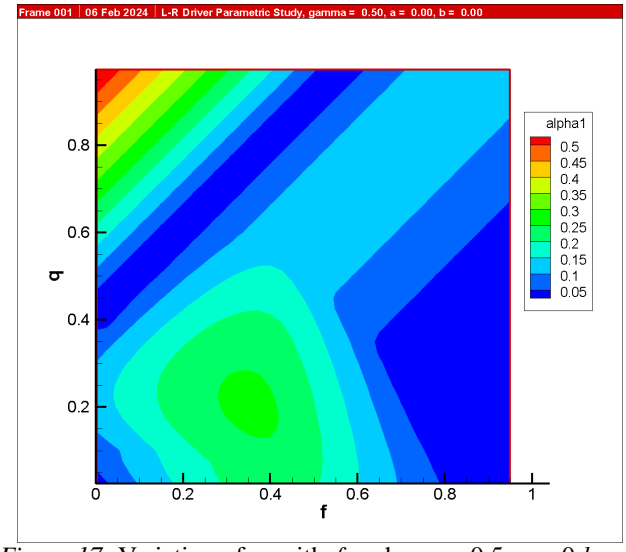

Figure 17. Variation of α_1 with f and q, $\gamma = 0.5$, $a = 0$ $b = 0$

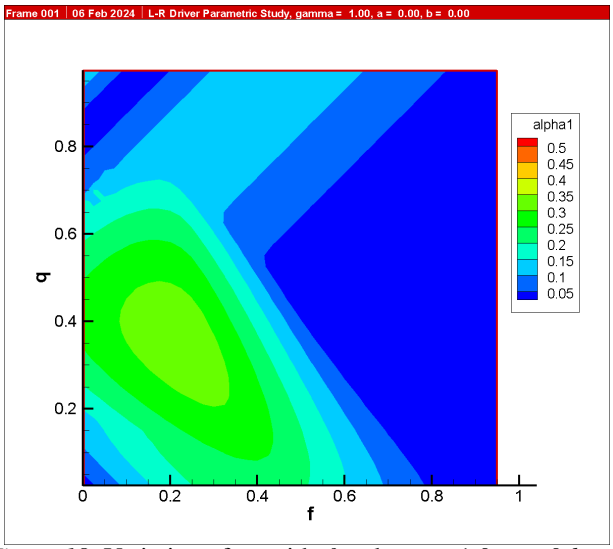

Figure 18. Variation of α_1 with f and q, $\gamma = 1.0$, $a = 0$ $b = 0$

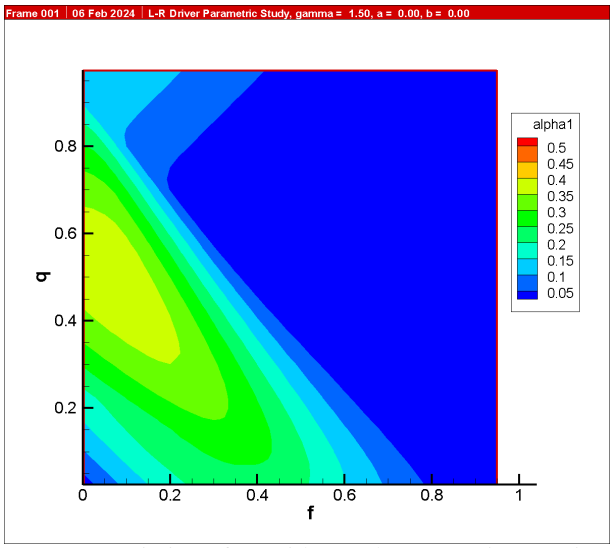

Figure 19. Variation of α_1 with f and q, $\gamma = 1.5$, $a = 0$ $b = 0$

Based on comparing the results of Figures 29-32 with those of Figures 33-36, there is no question that the purely longitudinal system advances with a lower power consumption. Optimisation of energy consumption with the advance of the pile is something that comes up frequently in Soviet literature on the subject, and this includes both vibratory and impact-vibration equipment. However, the vibratory or impact-vibratory equipment is not the only machine that is consuming energy on a construction site; it is entirely possible that the higher speed of driving will more than compensate for the increased energy requirements of the equipment actually sinking or extracting the pile. This is something that needs to be added to the discussion by D. Warrington (2021) on the subject of the difference between power consumption considerations in Soviet vs. other equipment.

Comparison of change of pile diameter

As a practical matter it is impossible, given the size variety of all types of tubular piles, to perfectly match the diameter of the pile with the rotational eccentric diameter, i.e., $a = 1$. For this reason it is necessary to take a look at different values of a for a constant $b = 1$, namely $a = 0.5$ (Figures 37 - 40) and $a = 1.5$ (Figures 41 - 44.) Values for $a = 1$ have already been presented in Figures 13 - 16.

The general result is that, as a increases, i.e., the diameter of the pile relative to the rotational eccentric diameter, $Y_{1_{max}}$ decreases, although this effect decreases with increasing toe

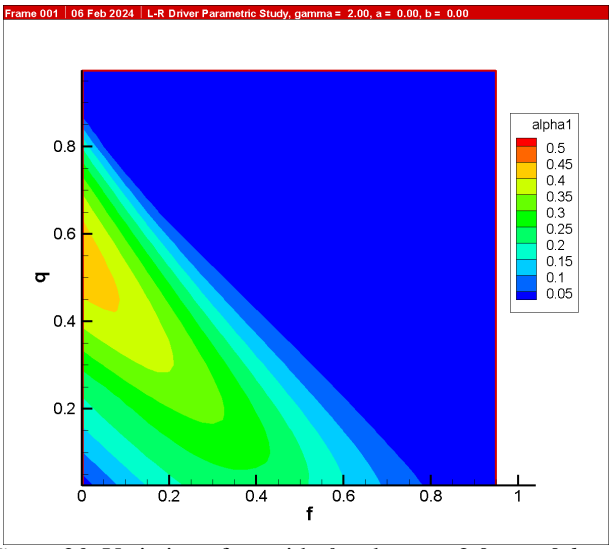

Figure 20. Variation of α_1 with f and q, $\gamma = 2.0$, $a = 0$ $b = 0$

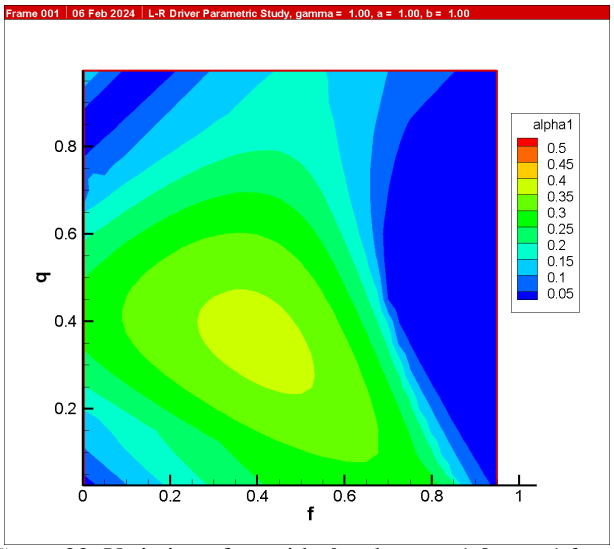

Figure 22. Variation of α_1 with f and q, $\gamma = 1.0$, $a = 1$ $b = 1$

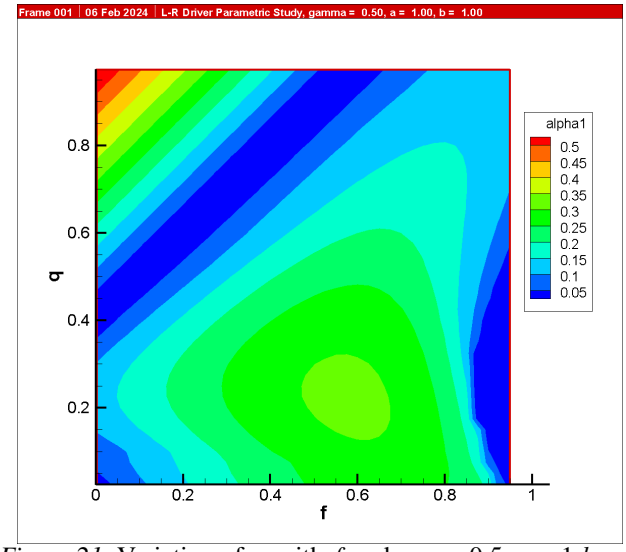

Figure 21. Variation of $\alpha_1$with f and q, $\gamma = 0.5$, $a = 1$ $b = 1$

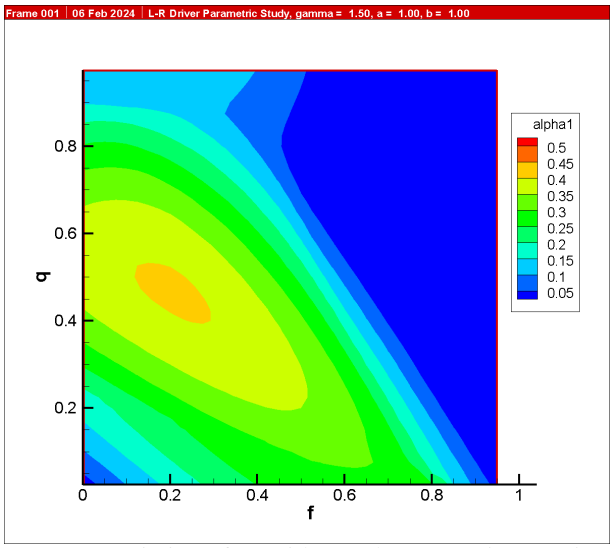

Figure 23. Variation of α_1 with f and q, $\gamma = 1.5$, $a = 1$ $b = 1$

resistance. One thing to keep in mind is that, as the diameter increases, barring size effects in the unit shaft friction, the shaft friction will increase with the perimeter (and thus the diameter) with the same soil and pile length. As $Y_{1_{max}}$ generally decreases with increasing f, this indicates a further deterioration in performance, and emphasises the importance of properly matching the equipment to the piles being driven.

Comparison of change of system rotational inertia

The last variation is of the variable b. This variable, given by Equation (33), is a rough measure of the ratio of the mass of the system times the system radii (pile and rotational eccentric) vs. the rotational mass moment of inertia of the system. As the latter increases, b decreases and with it the rotational amplitude of the system (see Equation (21). The effects of the change of b can be seen in Figure 8 for one case; the following will generalise the results. Holding $a = 1$, the case of $b = 1$ was shown in Figures 13 - 16. Results for $b = 0.25$ are shown in Figures 45 - 48 and for $b = 2$ in Figures 49 - 52.

The trends shown in this study are very similar to that shown in Figure 8. Although increasing b is important for the design of this equipment, it is one with diminishing returns. This is especially true as γ increases. As is always the case with pile driving equipment, the design of the equipment must balance its performance with durability and simplicity of construction in order for the machine to be economical both in initial purchase and during its useful life.

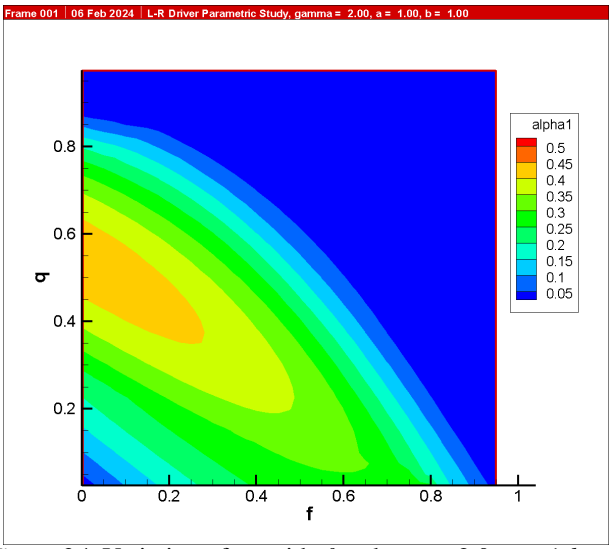

Figure 24. Variation of α_1 with f and q, $\gamma = 2.0$, $a = 1$ $b = 1$

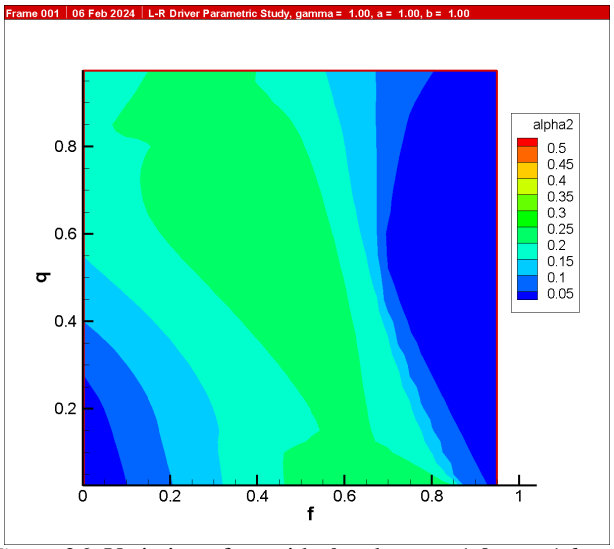

Figure 26. Variation of α_2 with f and q, $\gamma = 1.0$, $a = 1$ $b = 1$

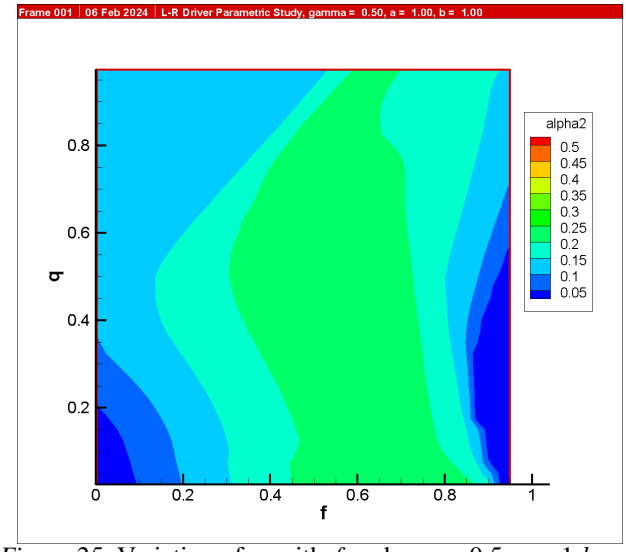

Figure 25. Variation of $\alpha_2$with f and q, $\gamma = 0.5$, $a = 1$ $b = 1$

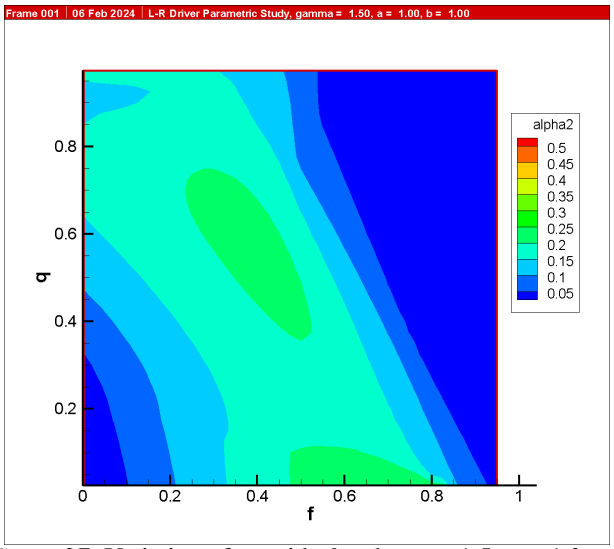

Figure 27. Variation of α_2 with f and q, $\gamma = 1.5$, $a = 1$ $b = 1$

Discussion

1. There is no question that the downward movement of the vibratory driver/pile system is greater with both longitudinal and rotational oscillations than with longitudinal ones alone. It is not more efficient from an energy standpoint relative to the system itself; however, energy efficiency must be considered in the context of the entire energy consumption on the job site, not just vibratory driving.

2. The relationship between downward motion and the speed of the driving was discussed in D. Warrington (2021) and is a function of the half-amplitude (Equation (20),) $Y_{1_{max}}$ and the frequency of vibrations ω.

3. Figures 7 and 8 show that $Y_{1_{max}}$ is greater using the model developed than that of Tseitlin et al. (1987). The character of the presentation of the latter makes the reason behind this uncertain.

4. Variations of a and b show that $Y_{1_{max}}$ decreases with increasing a and increases with increasing b. These should be taken into consideration when designing equipment for this application.

5. The optimisation program UNCMIN generally performed well. Although there was no necessity for the initial and final conditions of velocity be the same, in general the differences were small. Some of the graphs revealed anomalies in the results. It is possible that a derivative-free optimisation model such as the one used in D. C. Warrington (2016) may have resulted in superior matching, although such methods tend to be costly. Geotechnical problems in

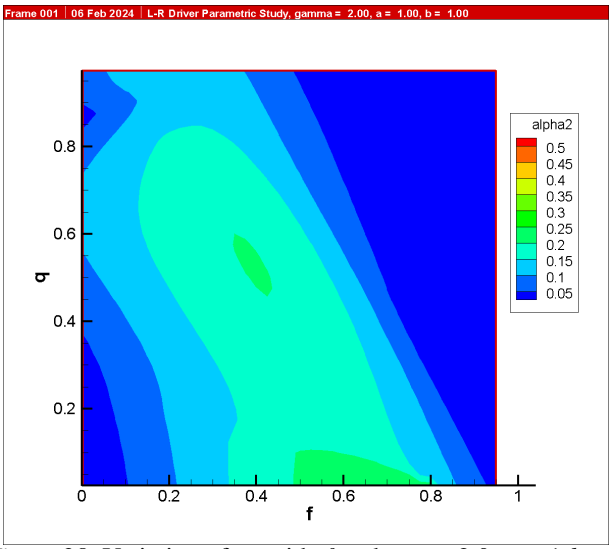

Figure 28. Variation of α_2 with f and q, $\gamma = 2.0$, $a = 1$ $b = 1$

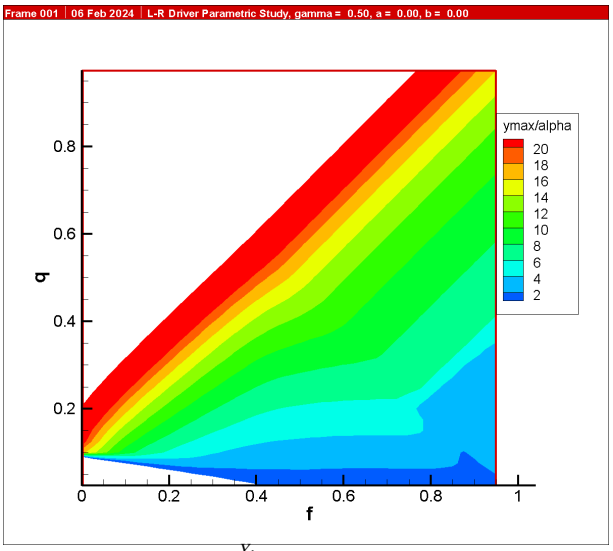

Figure 29. Variation of $\frac{Y_{1_{max}}}{\alpha_1}$ with f and q, $\gamma = 0.5$, $a = 0$ $b = 0$

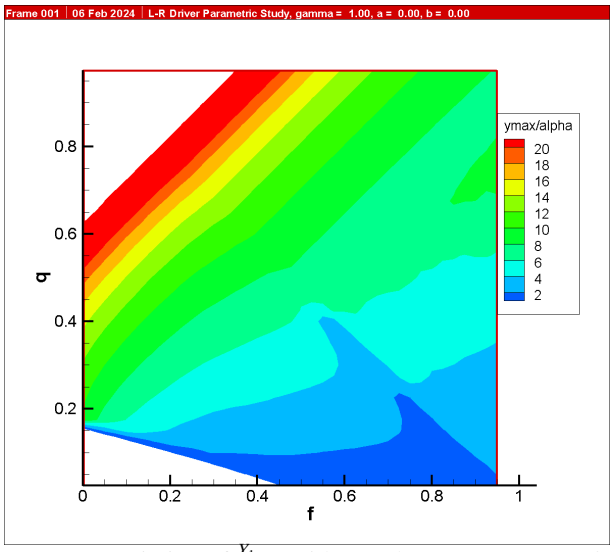

Figure 30. Variation of $\frac{Y_{1_{max}}}{\alpha_1}$ with f and q, $\gamma = 1.0$, $a = 0$ $b = 0$

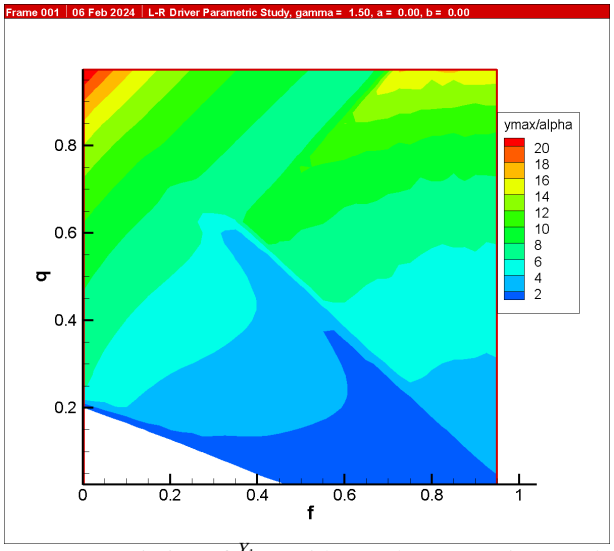

Figure 31. Variation of $\frac{Y_{1_{max}}}{\alpha_1}$ with f and q, $\gamma = 1.5$, $a = 0$ $b = 0$

general are discontinuously non-linear and frequently do not lend themselves well to Newton's Method-based solutions such as UNCMIN due to the danger of false minima. This explains, for example, why slope stability problems are commonly solved using grid optimisation. In spite of the difficulties, UNCMIN allowed the simulation of the steady-state condition with a single-cycle analysis, and using methods such as this may be promising for future analysis of both impact, vibratory and impact-vibratory driving of piles.

6. The inability to use the model to determine the phase angle α was an important drawback to the analysis, although in many cases the difference in $Y_{1_{max}}$ was small.

7. The need to get away from the purely Coulombic model of shaft friction and the purely plastic one of toe resistance is necessary both from the standpoint of proper modelling of the physical system and the difficulties of numerical simulation. Tseitlin et al. (1987) propose a model which is both elasto-plastic and reduces the resistance with breakthrough, but there is doubtless a better one. It is interesting to note that much of the Soviet effort to simulate vibratory pile driving–and to size drivers for specific applications, as was done by Savinov and Luskin (1960)–was done without consideration of the reduction of resistance due to movement of the soil, or strain softening.

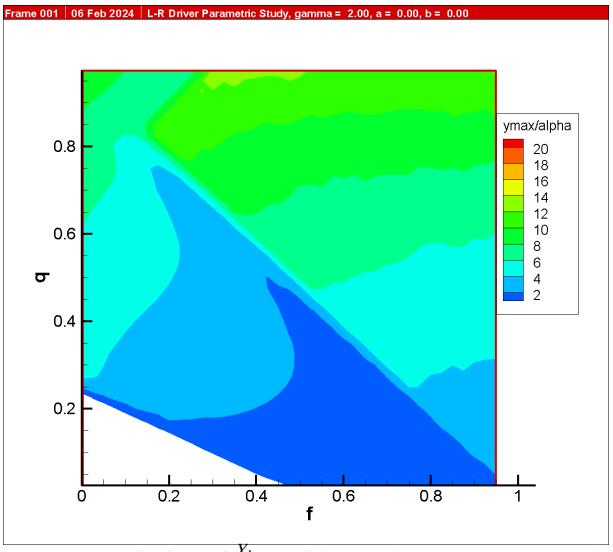

Figure 32. Variation of $\frac{Y_{1max}}{\alpha_1}$ with f and q, $\gamma = 2.0$, $a = 0$ $b = 0$

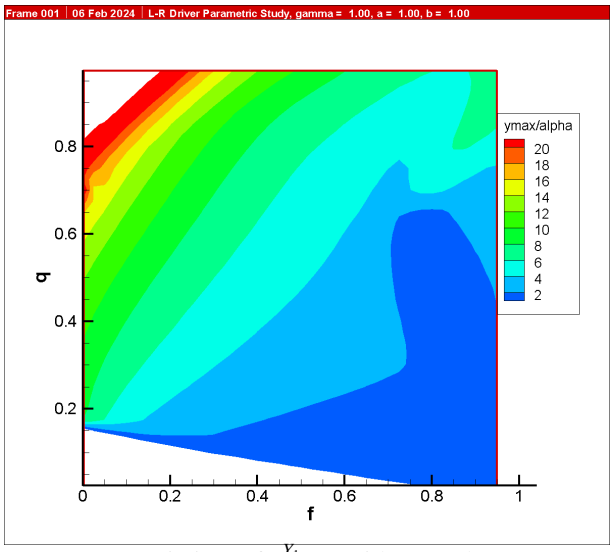

Figure 34. Variation of $\frac{Y_{1max}}{\alpha_1+\alpha_2}$ with f and q, $\gamma = 1.0$, $a = 1$ $b = 1$

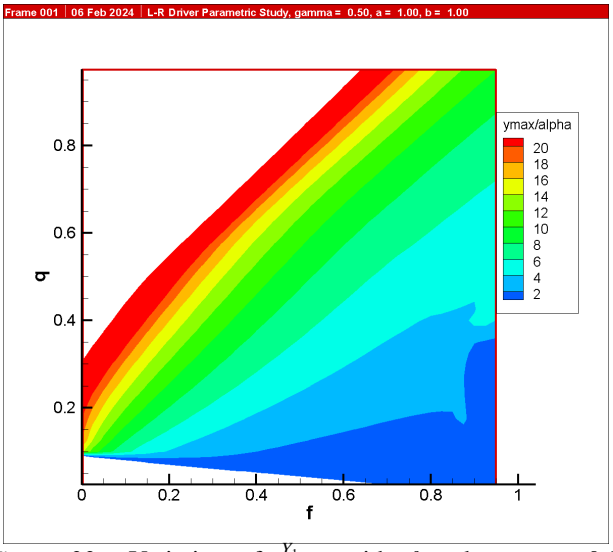

Figure 33. Variation of $\frac{Y_{1max}}{\alpha_1+\alpha_2}$ with f and q, $\gamma = 0.5$, $a = 1$ $b = 1$

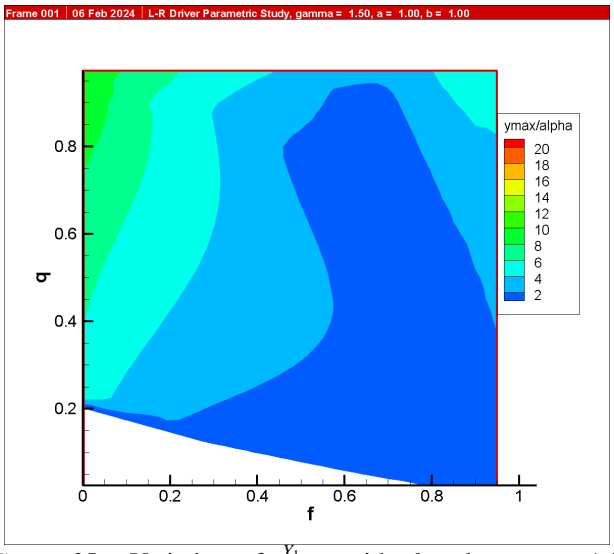

Figure 35. Variation of $\frac{Y_{1max}}{\alpha_1+\alpha_2}$ with f and q, $\gamma = 1.5$, $a = 1$ $b = 1$

Conclusion

The application of rotary oscillations in conjunction with longitudinal ones for driving axisymmetric piles results in improved performance and higher sinking speeds, based on the model used. In order to properly predict this performance and perhaps the axial capacity of these piles in use, a better soil model is necessary. This condition applies to virtually all vibratory pile driving, and so the search for a solution to this long-running problem will continue for the foreseeable future.

Nomenclature

α Phase angle, radians

γ Ratio of toe resistance to dynamic force

γ_{min} Minimum value of γ

ω Rotational frequency of eccentrics, rad/sec

$\Phi(\tau)$ Dimensionless rotational displacement as a function of dimensionless time

$\phi(t)$ Rotational displacement of vibrating system as a function of time, radians

τ Dimensionless time

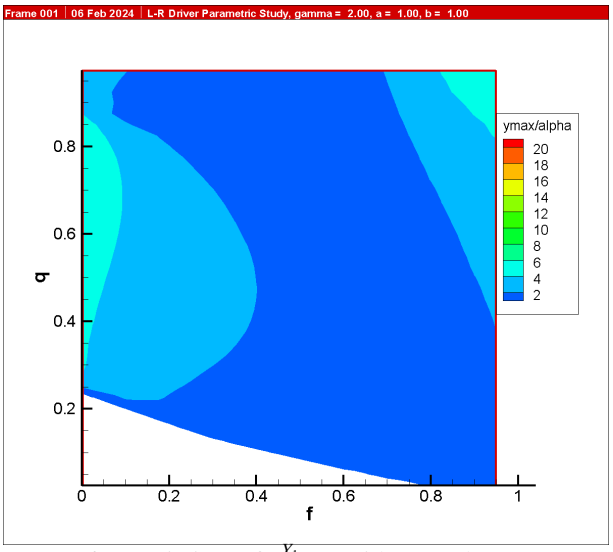

Figure 36. Variation of $\frac{Y_{1_{max}}}{\alpha_1+\alpha_2}$ with f and q, $\gamma = 2.0$, $a = 1$ $b = 1$

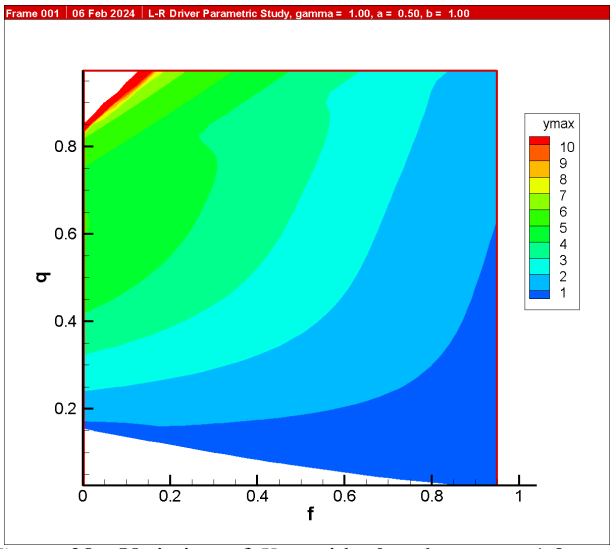

Figure 38. Variation of $Y_{1_{max}}$ with f and q, $\gamma = 1.0$, $a = 0.5$ $b = 1$

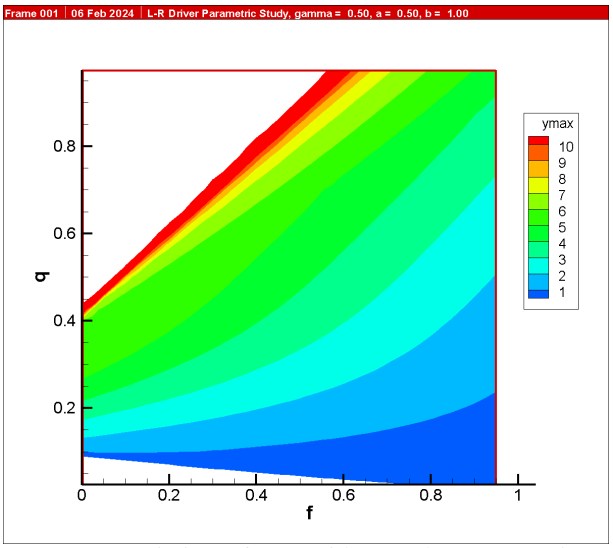

Figure 37. Variation of $Y_{1_{max}}$ with f and q, $\gamma = 0.5$, $a = 0.5$ $b = 1$

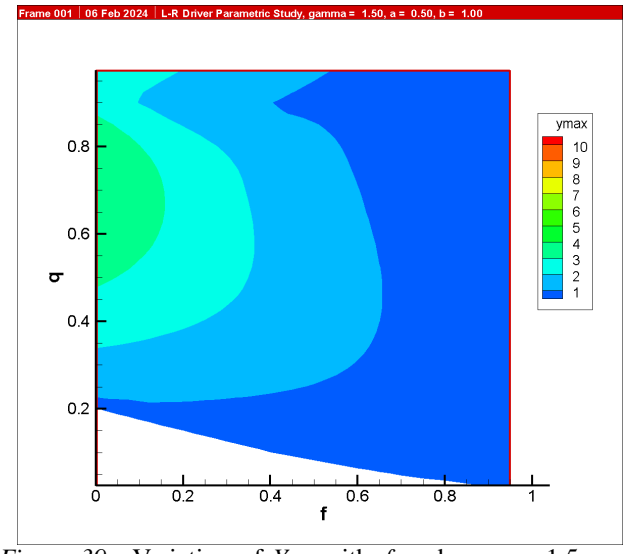

Figure 39. Variation of $Y_{1_{max}}$ with f and q, $\gamma = 1.5$, $a = 0.5$ $b = 1$

A Half-amplitude of longitudinal vibrations, m

a Ratio of pile radius to rotational eccentric radius

A_1 Half-amplitude of rotational oscillations, m

b Ratio of nominal rotational mass moment of inertia to actual mass moment of inertia

c_0 Rotational soil damping, N-m-sec/rad

C_1, C_2, C_3, C_4 Constants of integration

F Shaft resistance of pile during driving, N

f Ratio of shaft friction to dynamic force

F_1 Dimensionless Longitudinal Velocity

F_2 Dimensionless Rotational Acceleration

F_3 Dimensionless Rotational Velocity

F_4 Dimensionless Rotational Acceleration

f_f Coulombic coefficient of friction between the pile toe and the pile toe soil

I_0 Rotational mass moment of inertia, $kg - m^2$

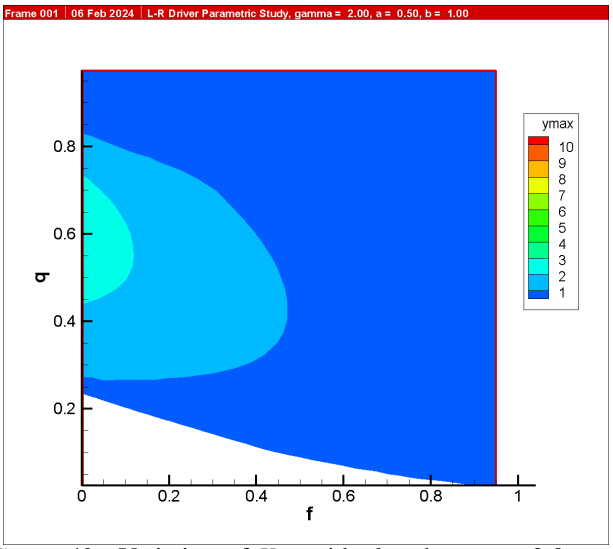

Figure 40. Variation of $Y_{1_{max}}$ with f and q, $\gamma = 2.0$, $a = 0.5$ $b = 1$

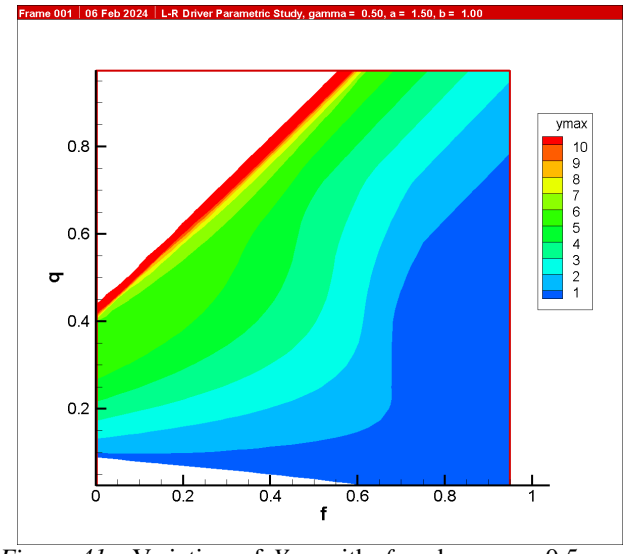

Figure 41. Variation of $Y_{1_{max}}$ with f and q, $\gamma = 0.5$, $a = 1.5$ $b = 1$

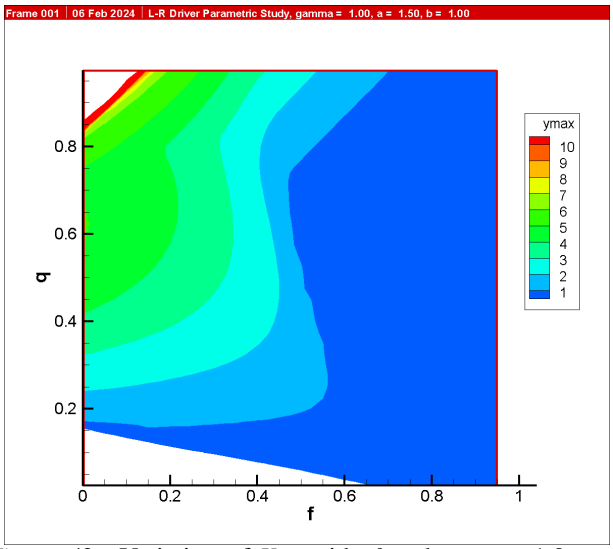

Figure 42. Variation of $Y_{1_{max}}$ with f and q, $\gamma = 1.0$, $a = 1.5$ $b = 1$

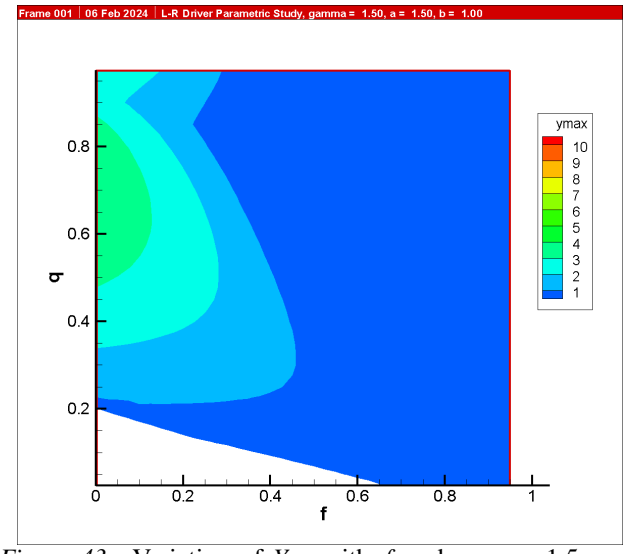

Figure 43. Variation of $Y_{1_{max}}$ with f and q, $\gamma = 1.5$, $a = 1.5$ $b = 1$

K Eccentric moment, kg-m

m Vibrating mass of system, kg

n_{con} Contact state of pile with toe soil

P_o Dynamic force of eccentrics, N

Q Weight of driving system (including static weight of suspension,) N

q Ratio of Q with P_o

R Toe resistance to driving, N

r Ouside radius of pile, m

r_1 Offset radius of eccentrics for rotational oscillation, m

t Time, seconds

v_0 Dimensionless longitudinal velocity at $\tau = 0$

$X(\tau)$ Dimensionless longitudinal displacement as a function of dimensionless time

$x(t)$ Displacement as a function of time, m

Y_1 Dimensionless Longitudinal Displacement

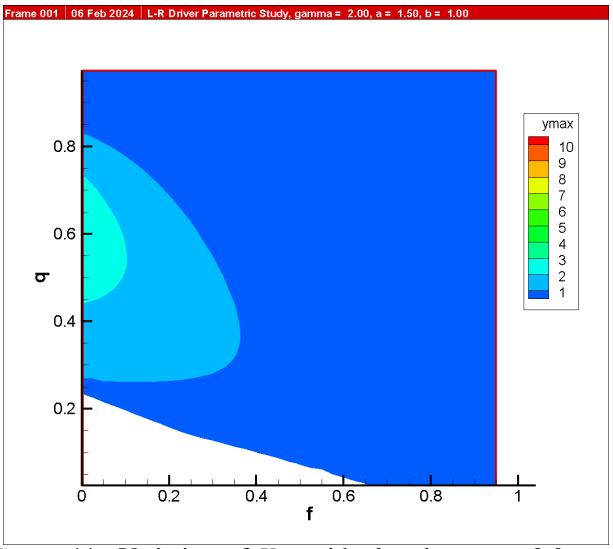

Figure 44. Variation of $Y_{1_{max}}$ with f and q, $\gamma = 2.0$, $a = 1.5$ $b = 1$

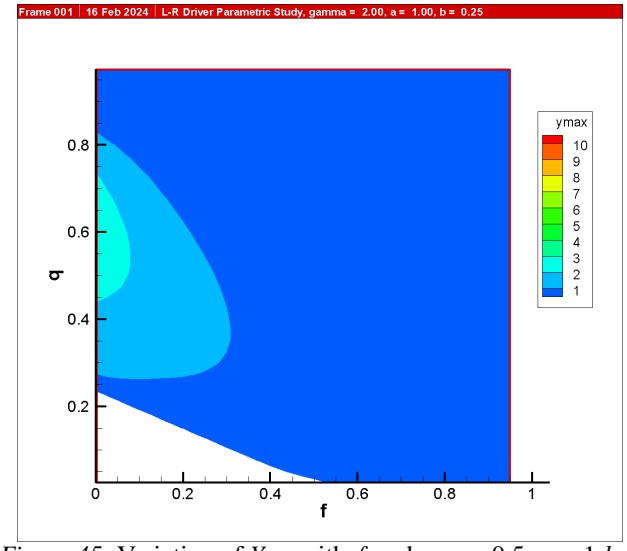

Figure 45. Variation of $Y_{1_{max}}$ with f and q, $\gamma = 0.5$, $a = 1$ $b = 0.25$

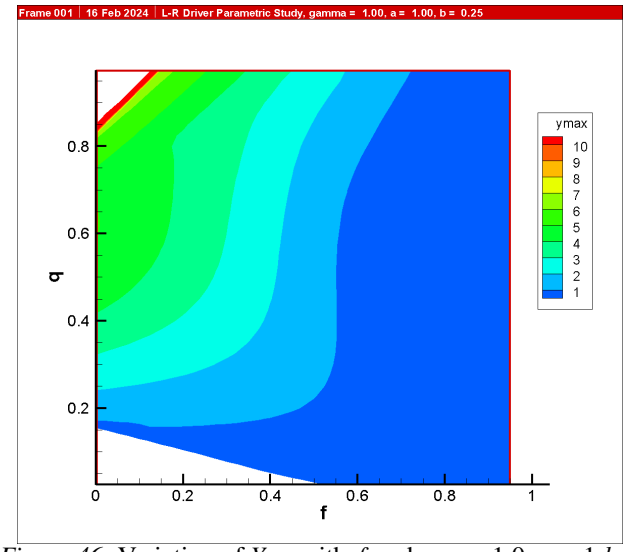

Figure 46. Variation of $Y_{1_{max}}$ with f and q, $\gamma = 1.0$, $a = 1$ $b = 0.25$

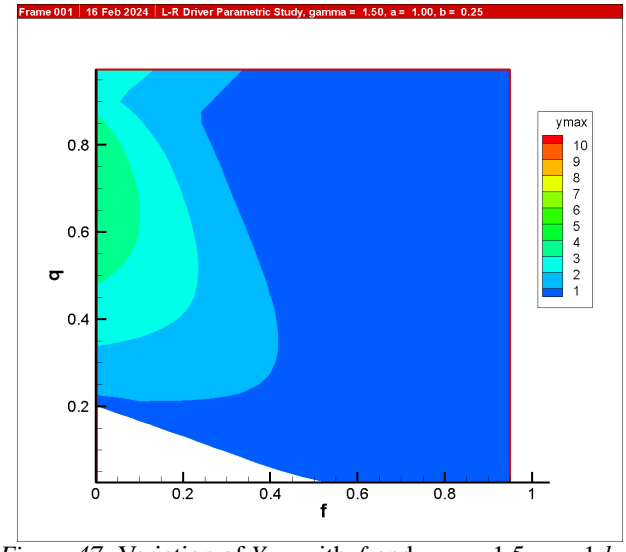

Figure 47. Variation of $Y_{1_{max}}$ with f and q, $\gamma = 1.5$, $a = 1$ $b = 0.25$

Y_{1max} Maximum Longitudinal Displacement at $\tau = 2\pi$

Y_2 Dimensionless Longitudinal Velocity

Y_3 Dimensionless Rotational Displacement

Y_4 Dimensionless Rotational Velocity

$\bar{\phi}(\tau)$ Rotational displacement as a function of dimensionless time, radians

$\bar{x}(\tau)$ Displacement as a function of τ, m

References

Barkan, D. (1957, August). Foundation and drilling by the vibration method. *Proceedings of the Fourth International Conference on Soil Mechanics and Foundation Engineering*, *2*, 3–7.

Carnahan, B., Luther, H., & Wilkes, J. (1969). *Applied numerical methods*. New York, NY: John Wiley & Sons, Inc.

Dennis, J., & Schnabel, R. (1996). *Numerical methods for unconstrained optimization and nonlinear equations*. Philadelphia: Society for Industrial and Applied Mathematics.

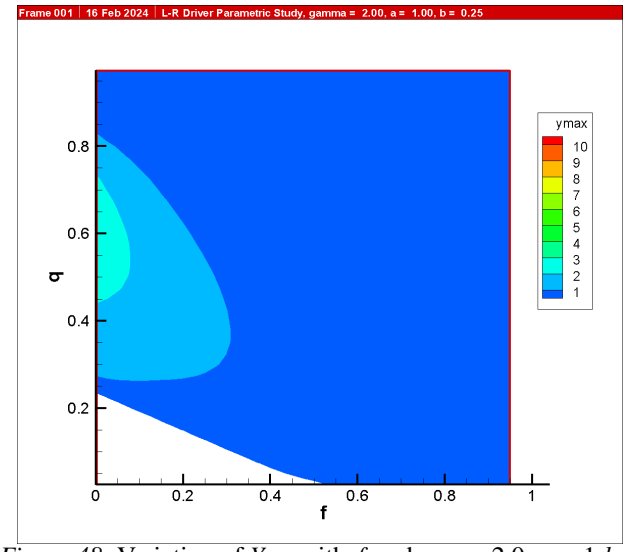

Figure 48. Variation of $Y_{1_{max}}$ with f and q, $\gamma = 2.0$, $a = 1$ $b = 0.25$

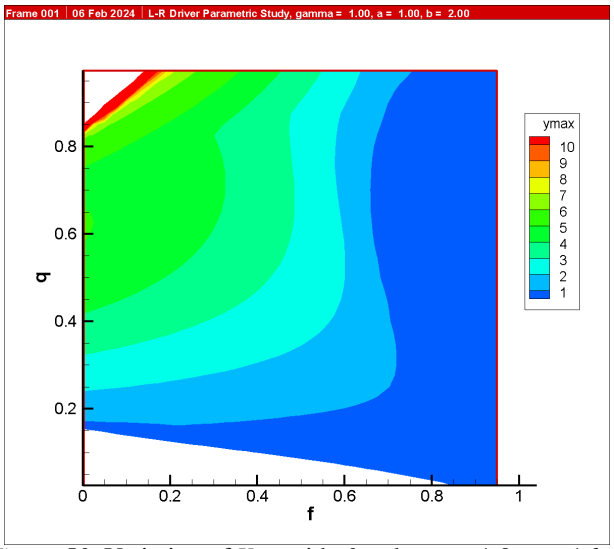

Figure 50. Variation of $Y_{1_{max}}$ with f and q, $\gamma = 1.0$, $a = 1$ $b = 2$

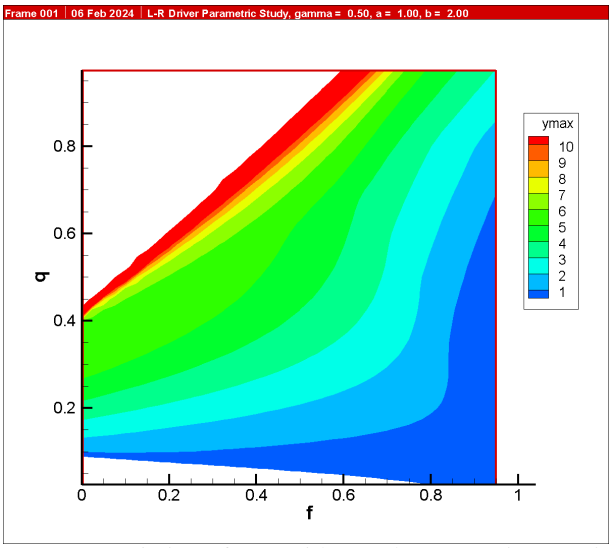

Figure 49. Variation of $Y_{1_{max}}$ with f and q, $\gamma = 0.5$, $a = 1$ $b = 2$

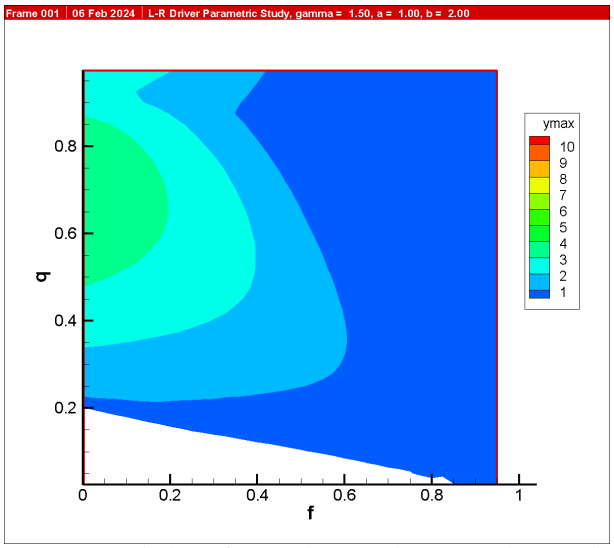

Figure 51. Variation of $Y_{1_{max}}$ with f and q, $\gamma = 1.5$, $a = 1$ $b = 2$

Massarsch, K. (2023). Soil resistance during vibratory driving in sand. *Proceedings of the Institution of Civil Engineers: Geotechnical Engineering,*. doi: 10.1680/jgeen.22.00193

Navy, U. (1986). *Foundations and earth structures* (Tech. Rep. No. DM 7.02). Arlington, VA: Naval Facilities Engineering Command.

Savinov, O., & Luskin, A. Y. (1960). *Vibratsionnyy metod pogruzheniya i yego primeneniye v stroitel'stve (the vibration method of driving piles and its use in construction)*. Leningrad, USSR: Gosstroyizdat.

Schnabel, R., Koontz, J., & Weiss, B. E. (1985, June). *A modular system of algorithms for unstrained minimization* (Tech. Rep.). University of Colorado at Boulder, Department of Computer Science.

Tseitlin, M. (1969, September). Sinking a cylindrical casing into the ground by means of lengthwise and rotary vibrations. *Osnovaniya, Fundamenty i Mekhanika Gruntov*(5), 19-22.

Tseitlin, M., Verstov, V., & Azbel, G. (1987). *Vibratsionnaya tekhnika i tekhnologiya v svainykh i burovikh rabotakh (vibratory methods and the technology of piling and boring work)*. Leningrad, USSR: Stroiizdat, Leningradskoe Otdelenie.

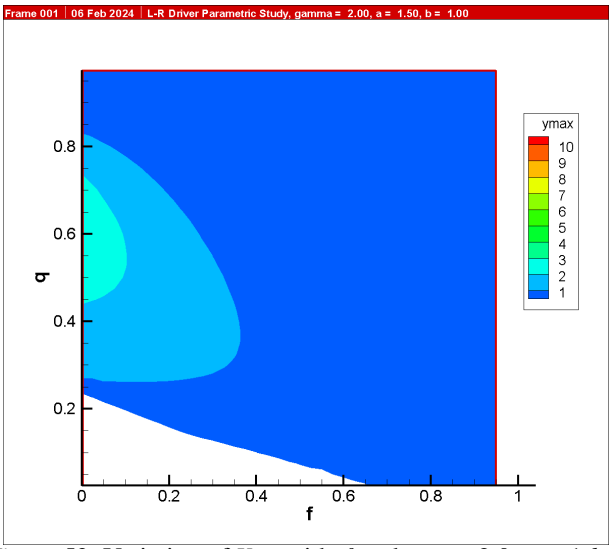

Figure 52. Variation of $Y_{1_{max}}$ with f and q, $\gamma = 2.0$, $a = 1$ $b = 2$

Tsetas, A., Tsouvalas, A., Gomez, S. S., Pisano, F., Kementzetzidis, E., Molenkamp, T., ... Metrikine, A. V. (2023). Gentle driving of piles (gdp) at a sandy site combining axial and torsional vibrations: Part i - installation tests. *Ocean Engineering*, *270*, 113453. doi: https://doi.org/10.1016/j.oceaneng.2022.113453

Warrington, D. (2006, September). Development of a parameter selection method for vibratory pile driver design with hammer suspension. *Colloquium of the Department of Mathematics of the University of Tennessee at Chattanooga*.

Warrington, D. (2021, April). *Reconstructing a soviet-era plastic model to predict vibratory pile driving performance* (Vol. 2021 ReSEARCH Dialogues Conference; Tech. Rep.). Chattanooga, TN: University of Tennessee at Chattanooga. doi: 10.13140/RG.2.2.30320.38403

Warrington, D. (2022, March). *Inclusion of rotational inertial effects in power consumption calculations for vibratory pile equipment* (Tech. Rep.). Chattanooga, TN: Affiliation: University of Tennessee at Chattanooga. doi: 10.13140/RG.2.2.30074.36805

Warrington, D. (2023). *Development of a parametric model for the simulation of impact-vibration pile driving equipment* (Tech. Rep.). University of Tennessee at Chattanooga. doi: 10.13140/RG.2.2.22395.18727

Warrington, D., & Erofeev, L. (1995, May). Russian impact-vibration pile driving equipment. *Pile Buck*, *May*(2), 4A-19B. Retrieved from `https://wp.me/p8QSbh-RF`

Warrington, D. C. (2016). *Improved methods for forward and inverse solution of the wave equation for piles* (Unpublished doctoral dissertation). University of Tennessee at Chattanooga, Chattanooga, TN.